



## Biogeochemical protocols and diagnostics for the CMIP6 Ocean Model Intercomparison Project (OMIP)

James C. Orr<sup>1</sup>, Raymond G. Najjar<sup>2</sup>, Olivier Aumont<sup>3</sup>, Laurent Bopp<sup>1</sup>, John L. Bullister<sup>4</sup>, Gokhan Danabasoglu<sup>5</sup>, Scott C. Doney<sup>6</sup>, John P. Dunne<sup>7</sup>, Jean-Claude Dutay<sup>1</sup>, Heather Graven<sup>8</sup>, Stephen M. Griffies<sup>7</sup>, Jasmin G. John<sup>7</sup>, Fortunat Joos<sup>9</sup>, Ingeborg Levin<sup>10</sup>, Keith Lindsay<sup>5</sup>, Richard J. Matear<sup>11</sup>, Galen A. McKinley<sup>12</sup>, Anne Mouchet<sup>13,14</sup>, Andreas Oschlies<sup>15</sup>, Anastasia Romanou<sup>16</sup>, Reiner Schlitzer<sup>17</sup>, Alessandro Tagliabue<sup>18</sup>, Toste Tanhua<sup>15</sup>, and Andrew Yool<sup>19</sup>

<sup>1</sup>LSCE/IPSL, Laboratoire des Sciences du Climat et de l'Environnement, CEA-CNRS-UVSQ, Gif-sur-Yvette, France

<sup>2</sup>Dept. of Meteorology and Atmospheric Science, Pennsylvania State University, University Park, Pennsylvania, USA

<sup>3</sup>Laboratoire d'Océanographie et de Climatologie: Expérimentation et Approches Numériques, IPSL, Paris, France

<sup>4</sup>Pacific Marine Environmental Laboratory, NOAA, Seattle, Washington, USA

<sup>5</sup>National Center for Atmospheric Research, Boulder, Colorado, USA

<sup>6</sup>Marine Chemistry & Geochemistry, Woods Hole Oceanographic Institution, Woods Hole, Massachusetts, USA

<sup>7</sup>NOAA Geophysical Fluid Dynamics Laboratory, Princeton, New Jersey, USA

<sup>8</sup>Dept. of Physics, Imperial College, London, UK

<sup>9</sup>Climate and Environmental Physics, Physics Inst. & Oeschger Center for Climate Change Res., Univ. of Bern, Bern, Switzerland

<sup>10</sup>Institut fuer Umweltphysik, Universitaet Heidelberg, Heidelberg, Germany

<sup>11</sup>CSIRO Oceans and Atmosphere, Hobart, Tasmania 7000, Australia

<sup>12</sup>Atmospheric and Oceanic Sciences, University of Wisconsin-Madison, Madison, Wisconsin, USA

<sup>13</sup>Max Planck Institute for Meteorology, Hamburg, Germany

<sup>14</sup>Astrophysics, Geophysics and Oceanography Department, University of Liege, Liege, Belgium

<sup>15</sup>GEOMAR Helmholtz Centre for Ocean Research Kiel, Kiel, Germany

<sup>16</sup>Columbia University and NASA-Goddard Institute for Space Studies, New York, NY, USA

<sup>17</sup>Alfred Wegener Institute, Bremerhaven, Germany

<sup>18</sup>Earth, Ocean and Ecological Sciences, University of Liverpool, Liverpool, UK

<sup>19</sup>National Oceanographic Centre, Southampton, UK

*Correspondence to:* James C. Orr (james.orr@lsce.ipsl.fr)

Received: 20 June 2016 – Discussion started: 18 July 2016

Revised: 28 February 2017 – Accepted: 7 March 2017 – Published: 9 June 2017

**Abstract.** The Ocean Model Intercomparison Project (OMIP) focuses on the physics and biogeochemistry of the ocean component of Earth system models participating in the sixth phase of the Coupled Model Intercomparison Project (CMIP6). OMIP aims to provide standard protocols and diagnostics for ocean models, while offering a forum to promote their common assessment and improvement. It also offers to compare solutions of the same ocean models when forced with reanalysis data (OMIP simulations) vs. when integrated within fully coupled Earth system models (CMIP6).

Here we detail simulation protocols and diagnostics for OMIP's biogeochemical and inert chemical tracers. These passive-tracer simulations will be coupled to ocean circulation models, initialized with observational data or output from a model spin-up, and forced by repeating the 1948–2009 surface fluxes of heat, fresh water, and momentum. These so-called OMIP-BGC simulations include three inert chemical tracers (CFC-11, CFC-12, SF<sub>6</sub>) and biogeochemical tracers (e.g., dissolved inorganic carbon, carbon isotopes, alkalinity, nutrients, and oxygen). Modelers will use their

preferred prognostic BGC model but should follow common guidelines for gas exchange and carbonate chemistry. Simulations include both natural and total carbon tracers. The required forced simulation (*omip1*) will be initialized with gridded observational climatologies. An optional forced simulation (*omip1-spinup*) will be initialized instead with BGC fields from a long model spin-up, preferably for 2000 years or more, and forced by repeating the same 62-year meteorological forcing. That optional run will also include abiotic tracers of total dissolved inorganic carbon and radiocarbon,  $C_T^{\text{abio}}$  and  $^{14}C_T^{\text{abio}}$ , to assess deep-ocean ventilation and distinguish the role of physics vs. biology. These simulations will be forced by observed atmospheric histories of the three inert gases and  $\text{CO}_2$  as well as carbon isotope ratios of  $\text{CO}_2$ . OMIP-BGC simulation protocols are founded on those from previous phases of the Ocean Carbon-Cycle Model Intercomparison Project. They have been merged and updated to reflect improvements concerning gas exchange, carbonate chemistry, and new data for initial conditions and atmospheric gas histories. Code is provided to facilitate their implementation.

## 1 Introduction

Centralized efforts to compare numerical models with one another and with data commonly lead to model improvements and accelerated development. The fundamental need for model comparison is fully embraced in Phase 6 of the Coupled Model Intercomparison Project (CMIP6), an initiative that aims to compare Earth system models (ESMs) and their climate-model counterparts as well as their individual components. CMIP6 emphasizes common forcing and diagnostics through 21 dedicated model intercomparison projects (MIPs) under a common umbrella (Eyring et al., 2016). One of these MIPs is the Ocean Model Intercomparison Project (OMIP). OMIP focuses on comparison of global ocean models that couple circulation, sea ice, and optional biogeochemistry, which together make up the ocean components of the ESMs used within CMIP6. OMIP works along two coordinated branches focused on ocean circulation and sea ice (OMIP-Physics) and on biogeochemistry (OMIP-BGC). The former is described in a companion paper in this same issue (Griffies et al., 2016), while the latter is described here.

Groups that participate in OMIP will use different ocean biogeochemical models coupled to different ocean general circulation models (OGCMs). The skill of the latter in simulating ocean circulation affects the ability of the former to simulate ocean biogeochemistry. Thus previous efforts to compare global-scale, ocean biogeochemical models have also strived to evaluate simulated patterns of ocean circulation. For instance, the Ocean Carbon-Cycle Model Intercomparison Project (OCMIP) included efforts to assess simulated circulation along with simulated biogeochemistry. OCMIP

began in 1995 as an effort to identify the principal differences between existing ocean carbon-cycle models. Its first phase (OCMIP1) included four models and focused on natural and anthropogenic components of oceanic carbon and radiocarbon (Sarmiento et al., 2000; Orr et al., 2001). OCMIP2 was launched in 1998, comparing 12 models with common biogeochemistry, and evaluating them with physical and inert chemical tracers (Doney et al., 2004; Dutay et al., 2002, 2004; Matsumoto et al., 2004; Orr et al., 2005; Najjar et al., 2007). In 2002, OCMIP3 turned its attention to evaluating simulated interannual variability in forced ocean biogeochemical models (e.g., Rodgers et al., 2004; Raynaud et al., 2006). More recently, OCMIP has focused on assessing ocean biogeochemistry simulated by ESMs (e.g., Bopp et al., 2013).

OCMIP2 evaluated simulated circulation using the physically active tracers, temperature  $T$  and salinity  $S$  (Doney et al., 2004), but also with passive tracers, i.e., those having no effect on ocean circulation. For example, OCMIP2 used two anthropogenic transient tracers, CFC-11 and CFC-12 (Dutay et al., 2002). Although these are reactive gases in the atmosphere that participate in the destruction of ozone, they remain inert once absorbed by the ocean. From an oceanographic perspective, they may be thought of as dye tracers given their inert nature and purely anthropogenic origin, increasing only since the 1930s (Fig. 1). Furthermore, precise measurements of CFC-11 and CFC-12 have been made throughout the world ocean, e.g., having been collected extensively during WOCE (World Ocean Circulation Experiment) and CLIVAR (Climate and Ocean – Variability, Predictability and Change). Hence they are well suited for model evaluation and are particularly powerful when used together to deduce decadal ventilation times of subsurface waters. Yet their combination is less useful to assess more recent ventilation, because their atmospheric concentrations have peaked and declined, since 1990 for CFC-11 and since 2000 for CFC-12, as a result of the Montreal Protocol. To fill this recent gap, oceanographers now also measure  $\text{SF}_6$ , another anthropogenic, inert chemical tracer whose atmospheric concentration has increased nearly linearly since the 1980s. Combining  $\text{SF}_6$  with either CFC-11 or CFC-12 is optimal for assessing even the most recent ventilation timescales. Together these inert chemical tracers can be used to assess transient time distributions. These TTDs are used to infer distributions of other passive tracer distributions, such as anthropogenic carbon (e.g., Waugh et al., 2003), which cannot be measured directly.

To help assess simulated circulation fields, OCMIP also included another passive tracer, radiocarbon, focusing on both its natural and anthropogenic components. Radiocarbon ( $^{14}\text{C}$ ) is produced naturally by cosmogenic radiation in the atmosphere, invades the ocean via air–sea gas exchange, and is mixed into the deep sea. Its natural component is useful because its horizontal and vertical gradients in the deep ocean result not only from ocean transport but

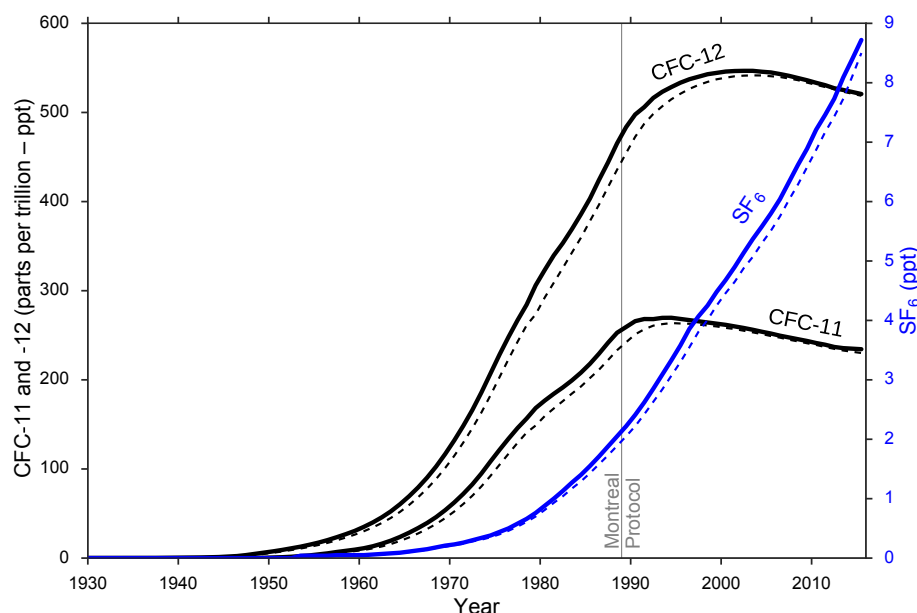


**Figure 1.** Histories of annual-mean tropospheric mixing ratios of CFC-11, CFC-12, and  $\text{SF}_6$  for the Northern Hemisphere (solid line) and Southern Hemisphere (dashed line). Mixing ratios are given in parts per trillion (ppt) from mid-year data provided by Bullister (2015). For the OMIP simulations, these inert chemical tracers need not be included until the fourth CORE-II forcing cycle when they will be initialized to zero on 1 January 1936 (at model date 1 January 0237). The vertical grey line indicates the date when the Montreal protocol entered into force.

also from radioactive decay (half-life of 5700 years), leaving a time signature for the slow ventilation of the deep ocean (roughly 100 to 1000 years depending on location). Hence natural  $^{14}\text{C}$  provides rate information throughout the deep ocean, unlike  $T$  and  $S$ . For example, the ventilation age of the deep North Pacific is about 1000 years, based on the depletion of its  $^{14}\text{C}/\text{C}$  ratio ( $-260\text{‰}$  in terms of  $\Delta^{14}\text{C}$ , i.e., the fractionation-corrected ratio relative to that of the preindustrial atmosphere) when compared with that of source waters from the surface Southern Ocean ( $-160\text{‰}$ ) (Toggweiler et al., 1989a). In the same vein, ventilation times of North Atlantic Deep Water and Antarctic Bottom Water have been deduced from  $^{14}\text{C}$  in combination with another biogeochemical tracer  $\text{PO}_4^*$  (“phosphate star”) (Broecker et al., 1998) by taking advantage of their strong regional contrasts. The natural component of radiocarbon complements the three inert chemical tracers mentioned above, which are used to assess more recently ventilated waters nearer to the surface. Yet the natural component is only half of the story.

During the industrial era, atmospheric  $\Delta^{14}\text{C}$  declined due to emissions of fossil  $\text{CO}_2$  (Suess effect) until the 1950s when that signal was overwhelmed by the much larger spike from atmospheric nuclear weapons tests (Fig. 2). Since the latter dominates, the total change from both anthropogenic effects is often referred to as bomb radiocarbon. As an anthropogenic transient tracer, bomb radiocarbon complements CFC-11, CFC-12, and  $\text{SF}_6$  because of its different atmospheric history and much longer air–sea equilibration time

(Broecker and Peng, 1974). Observations of bomb radiocarbon have been used to constrain the global-mean gas transfer velocity (Broecker and Peng, 1982; Sweeney et al., 2007); however, in recent decades, ocean radiocarbon changes have become more sensitive to interior transport and mixing, making it behave more like anthropogenic  $\text{CO}_2$  (Graven et al., 2012). Hence it is particularly relevant to use radiocarbon observations to evaluate ocean carbon-cycle models that aim to assess uptake of anthropogenic carbon as done during OCMIP (e.g., Orr et al., 2001).

Information from the stable carbon isotope  $^{13}\text{C}$  also helps to constrain the anthropogenic perturbation in dissolved inorganic carbon by exploiting the Suess effect (Quay et al., 1992, 2003). Driven by the release of anthropogenic  $\text{CO}_2$  produced from agriculture, deforestation, and fossil-fuel combustion, the Suess effect has resulted in a continuing reduction of the  $^{13}\text{C}/^{12}\text{C}$  ratio relative to that of the preindustrial atmosphere–ocean system. That ratio is reported relative to a standard as  $\delta^{13}\text{C}$ , which is not corrected for fractionation, unlike  $\Delta^{14}\text{C}$ . Fractionation occurs during gas exchange and photosynthesis, and  $\delta^{13}\text{C}$  is also sensitive to respiration of organic material and ocean mixing. Ocean  $\delta^{13}\text{C}$  observations have been used to test marine ecosystem models, including processes such as phytoplankton growth rate, iron limitation, and grazing (Schmittner et al., 2013; Tagliabue and Bopp, 2008) and may also provide insight into climate-related ecosystem changes. Past changes in  $\delta^{13}\text{C}$  recorded in

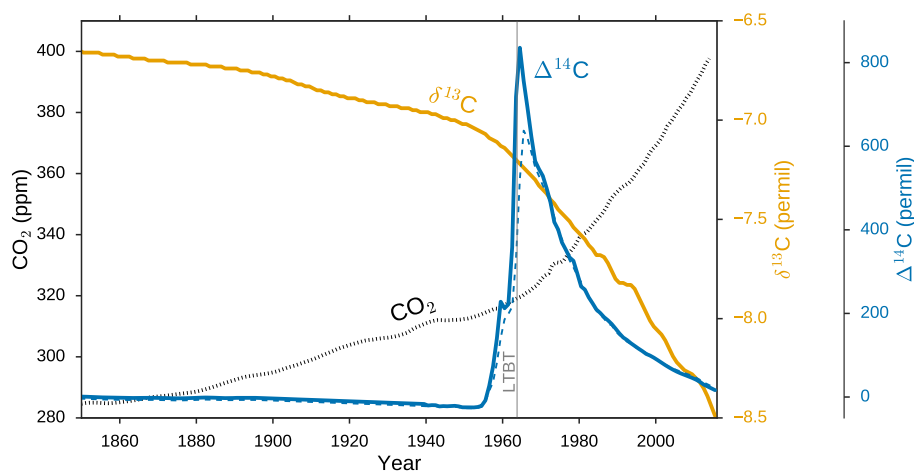


**Figure 2.** Annual-mean atmospheric histories for global-mean  $\text{CO}_2$  (black dots) and  $\delta^{13}\text{C}$  (orange) compared to hemispheric means of  $\Delta^{14}\text{C}$  for the north (blue solid) and south (blue dashes). Isotope records are available at input4mips (<https://esgf-node.llnl.gov/search/input4mips/>), including tropical  $\Delta^{14}\text{C}$  ( $30^\circ\text{S}$ – $30^\circ\text{N}$ ) (not shown). The  $\text{CO}_2$  data are identical to those used for CMIP6 (Meinshausen et al., 2016) and the carbon isotope data are common with C4MIP (Jones et al., 2016). The  $\text{CO}_2$  observations are from NOAA (Dlugokencky and Tans, 2016). The  $\delta^{13}\text{C}$  compilation uses ice-core and atmospheric measurements (Rubino et al., 2013; Keeling et al., 2001), while the  $\Delta^{14}\text{C}$  compilation uses tree-ring and atmospheric measurements Levin et al. (2010), extended after 2009 with unpublished data from the University of Heidelberg (I. Levin, personal communication, 2016). Post-2009 data are not needed in OMIP Phase 1, but will be used in subsequent phases. Between the beginning of the OMIP simulations on 1 January 1700 and the same date in 1850, the atmospheric concentrations of  $\text{CO}_2$ ,  $\delta^{13}\text{C}$ , and  $\Delta^{14}\text{C}$  are to be held constant at 284.32 ppm, 6.8, and 0‰, respectively. Also indicated are the preindustrial reference (0‰) for atmospheric  $\Delta^{14}\text{C}$  (horizontal grey dashed) and when the Limited Test Ban Treaty (LTBT) went into effect (vertical grey solid).

ice cores and marine sediments are likewise useful to evaluate models (Schmitt et al., 2012; Oliver et al., 2010).

Besides the aforementioned tracers to evaluate modeled circulation fields, OMIP-BGC also includes other passive tracers to compare simulated ocean biogeochemistry with data and among models, e.g., in terms of mean states, trends, and variability. Whereas all OCMIP2 groups used a common biogeochemical model (Najjar and Orr, 1998, 1999; Najjar et al., 2007), essentially testing its sensitivity to different circulation fields, OMIP will not adopt the same approach. Rather, OMIP focuses on evaluating and comparing preselected “combined” ocean models (circulation–ice–biogeochemistry) largely defined already by individual groups planning to participate in CMIP6. Those combined ocean models will be evaluated when forced by reanalysis data as well as when coupled within the CMIP6 ESMs.

OMIP-BGC model groups will use common physical forcing for ocean-only models and common formulations for carbonate chemistry, gas exchange, gas solubilities, and Schmidt numbers. Biogeochemical models will be coupled to the ocean–ice physical models, online (active and passive tracers will be modeled simultaneously), and they will be forced with the same atmospheric gas histories. Yet beyond those commonalities, model groups are free to choose their preferred ocean model configuration. For instance, groups may choose whether or not to include direct coupling between simulated chlorophyll and ocean dynamics. When coupled, chlorophyll is not a typical passive tracer; it is ac-

tive in the sense that it affects ocean circulation. Likewise, OMIP groups are free to use their preferred boundary conditions for the different sources of nutrients and micronutrients to the ocean via atmospheric deposition, sediment mobilization, and hydrothermal sources (e.g., for Fe) as well as lateral input of carbon from river and groundwater discharge. Biogeochemical models with riverine delivery of carbon and nutrients to the ocean usually include sediment deposition as well as loss of carbon from rivers back to the atmosphere through the air–sea exchange. Each group is free to use their preferred approach as long as mass is approximately conserved. Groups are requested to provide global integrals of these boundary conditions and to document their approach, preferably in a peer-reviewed publication.

OMIP-BGC aims to provide the technical foundation to assess trends, variability, and related uncertainties in ocean carbon and related biogeochemical variables since the onset of the industrial era and into the future. That foundation includes (1) the OMIP-BGC protocols for groups that will include inert chemical tracers and biogeochemistry in OMIP’s two forced global ocean model simulations, which couple circulation, sea ice, and biogeochemistry, and (2) the complete list of ocean biogeochemical diagnostics for OMIP, but also for CMIP6 (Eyring et al., 2016) and any ocean-related MIPs under its umbrella, e.g., C4MIP (Jones et al., 2016).

Simulated results from OMIP-BGC will be exploited to contribute to OMIP’s effort to study basic CMIP6 science questions on the origins and consequences of systematic

model biases. In particular, OMIP-BGC offers a forum for ocean biogeochemical modelers and a technical framework by which they will assess and improve biases of simulated tracer and biogeochemical components of CMIP6's ESMs. OMIP-BGC will contribute to the World Climate Research Programme's (WCRP) Grand Challenges by providing fundamental information needed to improve near-term climate prediction and estimates of carbon feedbacks in the climate system. Assessments will focus on current and future changes in ocean carbon uptake and storage, acidification, deoxygenation, and changes in marine productivity.

Novel analyses are expected from OMIP, in part because of recent improvements in the physical and biogeochemical components. For example, some of the physical models will have sufficient resolution to partially resolve mesoscale eddies. When coupled to biogeochemical models, that combination should allow OMIP to provide a first assessment of how air–sea CO<sub>2</sub> fluxes and related biogeochemical variables are affected by the ocean's intrinsic variability (also known as internal, chaotic, or unforced variability). Previous studies of the ocean's internal variability have focused only on physical variables (Penduff et al., 2011). Other studies have assessed the internal variability of ocean biogeochemistry, but they account only for the component associated with turbulence in the atmosphere. That is, they use a coarse-resolution ocean model coupled within an Earth system model framework (Lovenduski et al., 2016). Whether internal variability from the ocean works to enhance or reduce that from the atmosphere will depend on the variable studied, the region, and the model. OMIP aims to provide new insight into the ocean's contribution to internal variability while also quantifying the relative importance of the contribution of internal variability to the overall uncertainty of model projections.

## 2 Protocols

As described by Griffies et al. (2016), the OMIP-Physics simulations consist of forcing physical model systems (an ocean general circulation model coupled to a sea-ice model) with the interannually varying atmospheric data reanalysis known as the Coordinated Ocean-ice Reference Experiments (CORE-II) available over 1948–2009 (Large and Yeager, 2009). For OMIP, that 62-year forcing will be repeated five times to make simulations of 310 years. OMIP-BGC participants will make these simulations by coupling their prognostic models of ocean biogeochemistry, online, to their physical model systems. These OMIP-BGC simulations will be forced by observed records of atmospheric CO<sub>2</sub> and other gases during the 310-year period, defined as equivalent to calendar years 1700 to 2009. One 310-year OMIP simulation (*omip1*), with models initialized by data, is required (Tier 1) for all OMIP modeling groups; another 310-year simulation (*omip1-spunup*), with models initialized from a previous long spin-up simulation, is only for OMIP-BGC groups. Al-

though optional, the *omip1-spunup* simulation is strongly encouraged (Tier 2) to minimize drift, assess deep-ocean ventilation, and separate physical vs. biological components of ocean carbon. Details of these simulations are provided below.

The two forced ocean model simulations, *omip1* and *omip1-spunup*, differ from but are connected to the CMIP6 DECK and historical simulations. The only differences are the initialization and the forcing. In *omip1*, the ocean model is initialized with observations and forced by reanalysis data; in *historical*, the ocean model is coupled within an Earth system model framework after some type of spin-up. Likewise, the early portion of the *omip1-spunup* forced simulation is comparable to the CMIP6 DECK *piControl* coupled simulation. The complementarity of approaches will lead to a more thorough model evaluation.

When modeling chemical and biogeochemical tracers, it is recommended that OMIP groups use the same formulations for gas exchange and carbonate chemistry as outlined below. Little effort would be needed to modify code that is already consistent with previous phases of OCMIP. For gas exchange, model groups only need to change the value of the gas transfer coefficient, the formulations and coefficients for Schmidt numbers, and the atmospheric gas histories. For carbonate chemistry, groups should strive to use the constants recommended for best practices (Dickson et al., 2007) on the total pH scale and to avoid common modeling assumptions that lead to significant biases, notably an oversimplified alkalinity equation (Orr and Epitalon, 2015). Fortran 95 code to make these calculations is made available to OMIP-BGC participants.

### 2.1 Passive tracers

#### 2.1.1 Inert chemistry

The inert chemistry component of OMIP includes online simulation of CFC-11, CFC-12, and SF<sub>6</sub>. While CFC-12 is required (priority 1), CFC-11 and SF<sub>6</sub> are encouraged (priority 2). About the same amount of observational data in the global ocean exists for both CFC-11 and CFC-12, starting with early field programs in the 1980s. But CFC-12 has a longer atmospheric history, with its production starting a decade earlier (~1936) and a slower decline starting a decade later due to its longer atmospheric lifetime (112 vs. 52 years) relative to CFC-11 (Rigby et al., 2013). In contrast, SF<sub>6</sub> has continued to increase rapidly in recent decades. That increase will continue for many years despite ongoing efforts to restrict production and release of this potent greenhouse gas, because SF<sub>6</sub>'s atmospheric lifetime is perhaps 3000 years (Montzka et al., 2003). Using pairs of these tracers offers a powerful means to constrain ventilation ages; if model groups are only able to model two of these tracers, the ideal combination is CFC-12 and SF<sub>6</sub>.

Simulation protocols are based on the OCMIP2 design document (Najjar and Orr, 1998) and its ensuing CFC protocol (Orr et al., 1999a) and model comparison (Dutay et al., 2002). These inert passive tracers are computed online along with the active tracers (i.e., temperature and salinity in the physical simulation); they are independent of the biogeochemical model. OMIP models will be forced to follow historical atmospheric concentrations of CFC-11, CFC-12, and SF<sub>6</sub>, accounting for gas exchange and their different solubilities and Schmidt numbers. The same passive tracers should be included in the forced OMIP simulations and in the coupled CMIP6 historical simulations. Both types of simulations will be analyzed within the framework of OMIP. These inert chemistry tracers are complementary to the ideal age tracer that is included in the OMIP-Physics protocols (Griffies et al., 2016).

### 2.1.2 Biogeochemistry

For the other passive tracers, referred to as biogeochemistry, the OMIP-BGC protocols build on those developed for OCMIP. These include the OCMIP2 abiotic and biotic protocols (Najjar and Orr, 1998, 1999; Orr et al., 1999b) and the OCMIP3 protocols for interannually forced simulations (Aumont et al., 2004), all available online with links to code and data (see references) or as one combined PDF (see Supplement). Each model group will implement the OMIP protocol in their own prognostic ocean biogeochemical model as in OCMIP3, unlike the common-model approach of OCMIP2. Each OMIP biogeochemical model will be coupled online to an ocean general circulation model forced by the CORE-II atmospheric state. Geochemical boundary conditions for the atmosphere include an imposed constant atmospheric concentration of O<sub>2</sub> (mole fraction  $x_{O_2}$  of 0.20946) but a variable atmospheric CO<sub>2</sub> that follows observations (Meinshausen et al., 2016).

In addition, OMIP-BGC simulations should include a natural carbon tracer that sees a constant atmospheric mole fraction of CO<sub>2</sub> in dry air ( $x_{CO_2}$ ) fixed at the 1 January 1850 value (284.32 ppm), the CMIP6 preindustrial reference. This can be done either in an independent simulation with identical initial conditions and forcing, except for atmospheric  $x_{CO_2}$ , or in the same simulation by adding one or more new tracers to the biogeochemical model, referred to here as a *dual*- $C_T$  simulation. For this *dual* simulation, OMIP modelers would need to add a second dissolved inorganic carbon tracer ( $C_T^{nat}$ ), e.g., as in Yool et al. (2010). In OMIP, this added tracer will isolate natural CO<sub>2</sub> and keep track of model drift. Such *doubling* may also be necessary for other biogeochemical model tracers if they are directly affected by the CO<sub>2</sub> increase. For instance, expansion of the PISCES model (Aumont and Bopp, 2006) to a *dual*- $C_T$  implementation resulted in doubling not only of  $C_T$ , but also of its transported CaCO<sub>3</sub> tracer, which in turn affects total alkalinity  $A_T$  (Dufour et al., 2013). These natural tracers are referred to as

$C_T^{nat}$ , CaCO<sub>3</sub><sup>nat</sup>, and  $A_T^{nat}$ . Calculated variables affected by CO<sub>2</sub> should also be doubled, including pH,  $pCO_2$ , the air–sea CO<sub>2</sub> flux, and carbonate ion concentration. If biology depends on CO<sub>2</sub>, additional tracers such as nutrients and O<sub>2</sub> would also need to be doubled, making the doubling strategy less appealing. That strategy may also be more complex in some ESMs, e.g., if  $A_T$  changes abiotically due to warming-related changes in weathering and river runoff.

### 2.1.3 Abiotic carbon and radiocarbon

In the *omip1-spinup* simulation (as well as in its previously run spin-up) OMIP-BGC groups will also include two abiotic tracers to simulate total dissolved inorganic carbon  $C_T^{abio}$  and corresponding radiocarbon  $^{14}C_T^{abio}$ . These abiotic tracers do not depend on any biotic tracers. They should be included in addition to the biotic carbon tracers mentioned above ( $C_T$  and  $C_T^{nat}$ ). The ratio of the two abiotic tracers will be used to evaluate and compare models in terms of deep-ocean ventilation ages (natural radiocarbon) and near-surface anthropogenic invasion of bomb radiocarbon. In addition,  $C_T^{abio}$  will be compared to  $C_T$  to distinguish physical from biogeochemical effects on total carbon. For simplicity, simulations will be made abiotically following OCMIP2 protocols (Orr et al., 1999b). We recommend that participating groups add these two independent tracers to their biogeochemical model to simulate them simultaneously, thus promoting internal consistency while reducing costs.

In OMIP, we will use this two-tracer approach rather than the simpler approach of modeling only the  $^{14}C/C$  ratio directly (Toggweiler et al., 1989a, b). That simpler approach would be a better choice if our focus were only on comparing simulated and field-based estimates of the ocean's bomb- $^{14}C$  inventory, both of which are biased low (Naegler, 2009; Mouchet, 2013). The simpler modeling approach underestimates the inventory, because it assumes a constant air–sea CO<sub>2</sub> disequilibrium during the industrial era; likewise, field reconstructions of the ocean's bomb- $^{14}C$  inventory (Key et al., 2004; Peacock, 2004; Sweeney et al., 2007) are biased low because they assume that ocean  $C_T$  is unaffected by the anthropogenic perturbation. Yet in terms of oceanic  $\Delta^{14}C$ , the simple and two-tracer approaches yield similar results (Mouchet, 2013), because the effect of increasing  $C_T$  on oceanic  $\Delta^{14}C$  is negligible (Naegler, 2009). We also choose the two-tracer approach to take advantage of its  $C_T^{abio}$  tracer to help distinguish physical from biological contributions to  $C_T$ .

To model  $^{14}C$ , OMIP neglects effects due to fractionation (i.e., from biology and gas exchange). Hence model results will be directly comparable to measurements reported as  $\Delta^{14}C$ , a transformation of the  $^{14}C/C$  ratio designed to correct for fractionation (Toggweiler et al., 1989a). Thus biases associated with our abiotic approach may generally be neglected. For natural  $^{14}C$ , Bacastow and Maier-Reimer (1990) found essentially identical results for simulations that

accounted for biological fractionation vs. those that did not, as long as the atmospheric  $\text{CO}_2$  boundary conditions were identical. For bomb  $^{14}\text{C}$ , which also includes the Suess effect, neglecting biological fractionation results in small biases (Joos et al., 1997).

Hence for the *omip1-spunup* simulation, OMIP-BGC groups will simulate four flavors of dissolved inorganic carbon: biotic natural ( $C_T^{\text{nat}}$ ), biotic total ( $C_T$ ), abiotic total ( $C_T^{\text{abio}}$ ), and abiotic radiocarbon ( $^{14}C_T^{\text{abio}}$ ). Conversely for the *omip1* simulation, groups will simulate only the first two flavors,  $C_T^{\text{nat}}$  and  $C_T$ . These tracers may be simulated simultaneously or in separate simulations, although we recommend the former.

#### 2.1.4 Carbon-13

Groups that have experience modeling  $^{13}\text{C}$  in their biogeochemical model are requested to include it as a tracer in the OMIP-BGC simulations. Groups without experience should avoid adding it. It is not required to simulate  $^{13}\text{C}$  in order to participate in OMIP. Modeling groups that will simulate ocean  $^{13}\text{C}$  are requested to report net air–sea fluxes of  $^{13}\text{CO}_2$  and concentrations of total dissolved inorganic carbon-13 ( $^{13}C_T$ ) for the *omip1-spunup* simulation. In Sect. 2.5 we recommend how isotopic fractionation during gas exchange should be modeled. Carbon-13 is typically included in ocean models as a biotic variable influenced by fractionation effects during photosynthesis that depend on growth rate and phytoplankton type; some models also include fractionation during calcium carbonate formation (e.g., Tagliabue and Bopp, 2008). Modeling groups should incorporate ecosystem fractionation specific to their ecosystem model formulation. We do not request that modeling groups report variables related to  $^{13}\text{C}$  in phytoplankton or other organic carbon pools, only  $^{13}C_T$  and net air–sea  $^{13}\text{CO}_2$  fluxes.

#### 2.2 Duration and initialization

As described by Griffies et al. (2016), the physical components of the models are to be forced over 310 years, i.e., over five repeated forcing cycles of the 62-year CORE-II forcing (1948–2009). The biogeochemistry should be included, along with the physical system, during the full 310 years (1700–2009) and the inert chemistry only during the last 74 years (1936–2009). The biogeochemical simulations will be initialized on calendar date 1 January 1700, at the start of the first CORE-II forcing cycle. The inert anthropogenic chemical tracers (CFC-11, CFC-12,  $\text{SF}_6$ ) will be initialized to zero on 1 January 1936, during the fourth CORE-II forcing cycle at model date 1 January 0237.

For the *omip1* simulation, biogeochemical tracers will be initialized generally with observational climatologies. Fields from the 2013 World Ocean Atlas (WOA2013) will be used to initialize model fields of oxygen (Garcia et al., 2014a) as well as nitrate, total dissolved inorganic phosphorus, and to-

tal dissolved inorganic silicon (Garcia et al., 2014b). The latter two nutrients are often referred to simply as phosphate and silicate, but other inorganic P and Si species also contribute substantially to each total concentration (Fig. 3). Indeed it is the total dissolved concentrations ( $P_T$  and  $Si_T$ ) that are both modeled and measured. OMIP will provide all these initial biogeochemical fields by merging WOA2013's means for January, available down to 500 m (for nitrate, phosphate, and silicate), and down to 1500 m for oxygen, with its annual-mean fields below.

Model fields for  $A_T$  and preindustrial  $C_T$  will be initialized with gridded data from version 2 of the Global Ocean Data Analysis Project (GLODAPv2) from Lauvset et al. (2016), based on discrete measurements during WOCE and CLIVAR (Olsen et al., 2016). For greater consistency with GLODAPv1, OMIP-BGC model groups will use the  $C_T$  and  $A_T$  fields from GLODAPv2's first period (1986–1999, the WOCE era).

To initialize modeled dissolved organic carbon (DOC), OMIP provides fields from the adjoint model from Schlitzer (Hansell et al., 2009). For dissolved iron (Fe), OMIP simulations will not be initialized from observations because a full-depth, global 3-D data climatology is unavailable due to lack of data coverage, particularly in the deep ocean. Hence for initial Fe fields, OMIP provides the median model result from the Iron Model Intercomparison Project (FeMIP, Tagliabue et al., 2016). Yet that initialization field may not be well suited for all Fe models, which differ greatly. Although OMIP provides initialization fields for Fe and DOC, their actual initialization is left to the discretion of each modeling group. In a previous comparison (Kwiatkowski et al., 2014), groups did not initialize modeled Fe with a common field or approach because the complexity of the Fe cycle differed greatly between models. Likewise, there was no common approach to initialize DOC because biogeochemical models vary greatly in the way they represent its lability. Initialization of other tracers is less critical (e.g., phytoplankton biomass is restricted to the top 200 m and equilibrates rapidly, as do other biological tracers).

The *omip1* simulation is relatively short and is thus manageable by all groups, but many of its tracers will have large drifts because model initial states will be far from their equilibrium states. These drifts complicate assessment of model performance based on model–data agreement (Séférian et al., 2016). Hence a complementary simulation, *omip1-spunup*, is proposed, where biogeochemical tracers are initialized instead with a near-equilibrium state. Model groups may generate this spun-up initial state by any means at their disposal. The classic approach would be to spin up the model. That could be done either online, repeating many times the same physical atmospheric forcing (CORE-II), or offline, repeatedly cycling the physical transport fields from a circulation model forced by a single loop of the CORE-II forcing.

If the spin-up simulation is made online, groups should reset their model's physical fields at the end of every fifth cy-



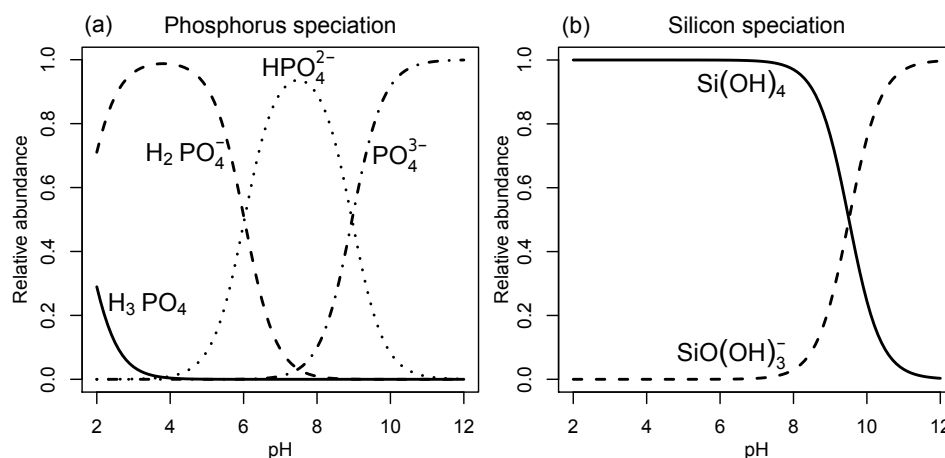


**Figure 3.** Relative molar abundance of inorganic species of phosphorus (left) and silicon (right) as a function of pH (total scale) in seawater at a temperature of 18 °C and salinity of 35.

cle of CORE-II forcing to their state at the beginning of the previous third cycle. Thus groups will avoid long-term drift in the model's physical fields, and the latter will not diverge greatly from those of the *ocmip1* simulation but be allowed to evolve freely over a period roughly equivalent to that of the transient  $\text{CO}_2$  increase (last three forcing cycles). Conversely, biogeochemical fields should not be reset. The end of the spin-up simulation will be reached only after many repetitions of the five consecutive forcing cycles with the online model. That final state (i.e., the physical and biogeochemical fields from the end of the final fifth cycle) will be used to initialize the *ocmip1-spinup* simulation. Offline spin-up simulations should be performed in a consistent fashion. That is, groups should first integrate their circulation model over two cycles of forcing and then use the physical circulation fields generated during the third forcing cycle to subsequently drive their offline biogeochemical model, typically until they reach the criteria described below.

If possible, the spin-up should be run until it reaches the biogeochemical equilibrium criteria adopted for OCMIP2. These criteria state that the globally integrated, biotic and abiotic air–sea  $\text{CO}_2$  fluxes ( $F_{\text{CO}_2}$  and  $F_{\text{CO}_2}^{\text{abio}}$ ) should each drift by less than  $0.01 \text{ Pg C year}^{-1}$  (Najjar and Orr, 1999; Orr et al., 1999b) and that abiotic  $^{14}\text{C}_\text{T}$  should be stabilized to the point that 98 % of the ocean volume has a drift of less than  $0.001 \text{ ‰ year}^{-1}$  (Aumont et al., 1998). The latter is equivalent to a drift of about 10 years in the  $^{14}\text{C}$  age per 1000 years of simulation. For most models, these drift criteria can be reached only after integrations of a few thousand model years. To reach the spun-up state with the classic approach, i.e., with the online or offline methods outlined above, we request that groups spin up their model for at least 2000 years, if at all possible. Other approaches to obtain the spun-up state, such as using tracer-acceleration techniques or fast solvers (Li and Primeau, 2008; Khatiwala,

2008; Merlis and Khatiwala, 2008), are also permissible. If used, they should also be applied until models meet the same equilibrium criteria described above.

The spin-up simulation itself should be initialized as for the *ocmip1* simulation, except for the abiotic tracers and the  $^{13}\text{C}_\text{T}$  tracer. The abiotic initial fields of  $A_\text{T}^{\text{abio}}$  and  $C_\text{T}^{\text{abio}}$  will be provided, being derived from initial fields of  $T$  and  $S$ . Although  $C_\text{T}^{\text{abio}}$  is a passive tracer carried in the model,  $A_\text{T}^{\text{abio}}$  is not. The latter will be calculated from the initial 3-D salinity field as detailed below; then that calculated field will be used to compute  $C_\text{T}^{\text{abio}}$  throughout the water column assuming equilibrium with the preindustrial level of atmospheric  $\text{CO}_2$  at the initial  $T$  and  $S$  conditions (using OMIP's carbonate chemistry routines). For  $^{14}\text{C}_\text{T}^{\text{abio}}$ , initial fields will be based on those from GLODAPv1 for natural  $\Delta^{14}\text{C}$  (Key et al., 2004). OMIP will provide these initial fields with missing grid cells filled based on values from adjacent ocean grid points. Groups that include  $^{13}\text{C}_\text{T}$  in *ocmip1-spinup* should initialize that in the precursor spin-up simulation to 0‰ following the approach of Jahn et al. (2015). Beware though that equilibration timescales for  $^{13}\text{C}$  are longer than for  $C_\text{T}$ , implying the need for a much longer spin-up.

### 2.3 Geochemical atmospheric forcing

The atmospheric concentration histories of the three inert chemical tracers (CFC-11, CFC-12, and  $\text{SF}_6$ ) to be used in OMIP are summarized by Bullister (2015) and shown in Fig. 1. Their atmospheric values are to be held to zero for the first three cycles of the CORE-II forcing, then increased starting on 1 January 1936 (beginning of model year 0237) according to the OMIP protocol. To save computational resources, the inert chemical tracers may be activated only from 1936 onward, starting from zero concentrations in the atmosphere and ocean. The atmospheric  $\text{CO}_2$  history used to force the OMIP models is the same as that used for



the CMIP6 historical simulation (Meinshausen et al., 2016), while carbon isotope ratios ( $\Delta^{14}\text{C}$  and  $\delta^{13}\text{C}$ ) are the same as those used by C4MIP (Jones et al., 2016). These atmospheric records of  $\text{CO}_2$  and carbon isotope ratios (Fig. 2) and those for the inert chemical tracers will be available at input4mips (<https://esgf-node.llnl.gov/search/input4mips>). The biogeochemical tracers are to be activated at the beginning of the 310-year simulation (on 1 January 1700) but initialized differently as described above for *omip1* and *omip1-spinup*. The atmospheric concentration of  $\text{CO}_2$  is to be maintained at the CMIP6 preindustrial reference of  $x\text{CO}_2^{\text{atm}} = 284.32$  ppm between calendar years 1700.0 and 1850.0, after which it must increase following observations (Meinshausen et al., 2016). The increasing  $x\text{CO}_2^{\text{atm}}$  will thus affect  $C_{\text{T}}$  but not  $C_{\text{T}}^{\text{nat}}$ , which sees only the preindustrial reference level of  $x\text{CO}_2^{\text{atm}}$ . The increasing  $x\text{CO}_2^{\text{atm}}$  is also seen by  $^{13}\text{C}_{\text{T}}$  and the two abiotic tracers,  $C_{\text{T}}^{\text{abio}}$  and  $^{14}\text{C}_{\text{T}}^{\text{abio}}$ , to be modeled only in the *omip1-spinup* simulation and its spin-up, the latter of which imposes a constant preindustrial  $x\text{CO}_2^{\text{atm}}$ .

## 2.4 Conservation equation

The time evolution equation for all passive tracers is given by

$$\frac{\partial C}{\partial t} = L(C) + J_C, \quad (1)$$

where  $C$  is the tracer concentration;  $L$  is the 3-D transport operator, which represents effects due to advection, diffusion, and convection; and  $J_C$  is the internal source–sink term. Conservation of volume is assumed in Eq. (1) and standard units of  $\text{mol m}^{-3}$  are used for all tracers. For the inert chemical tracers (CFC-11, CFC-12, and  $\text{SF}_6$ ),  $J_C = 0$ . For the abiotic carbon tracers, in the *omip1-spinup* simulation and its spin-up, the same term is also null for the total carbon tracer  $C_{\text{T}}$

$$J_{C_{\text{T}}^{\text{abio}}} = 0, \quad (2)$$

but not for the total radiocarbon tracer  $^{14}\text{C}_{\text{T}}^{\text{abio}}$  due to radioactive decay

$$J_{^{14}\text{C}_{\text{T}}^{\text{abio}}} = -\lambda ^{14}\text{C}_{\text{T}}^{\text{abio}}, \quad (3)$$

where  $\lambda$  is the radioactive decay constant for  $^{14}\text{C}$ , i.e.,

$$\lambda = \ln(2)/5700 \text{ years} = 1.2160 \times 10^{-4} \text{ years}^{-1}, \quad (4)$$

converted to  $\text{s}^{-1}$  using the number of seconds per year in a given model. For other biogeochemical tracers  $J_C$  is non-zero and often differs between models. For  $^{13}\text{C}_{\text{T}}$ ,  $J_C$  includes isotopic fractionation effects.

## 2.5 Air–sea gas exchange

Non-zero surface boundary conditions must also be included for all tracers that are affected by air–sea gas exchange: CFC-11, CFC-12,  $\text{SF}_6$ , dissolved  $\text{O}_2$ , and dissolved inorganic carbon in its various modeled forms ( $C_{\text{T}}$ ,  $C_{\text{T}}^{\text{nat}}$ ,  $C_{\text{T}}^{\text{abio}}$ ,  $^{14}\text{C}_{\text{T}}^{\text{abio}}$ ,

and  $^{13}\text{C}_{\text{T}}$ ). In OCMIP2, surface boundary conditions also included a virtual-flux term for some biogeochemical tracers, namely in models that had a virtual salt flux because they did not allow water transfer across the air–sea interface. Water transfer calls for different implementations depending on the way the free surface is treated, as discussed extensively by Roulet and Madec (2000). Groups that have implemented virtual fluxes for active tracers ( $T$  and  $S$ ) should follow the same practices to deal with virtual fluxes of passive tracers such as  $C_{\text{T}}$  and  $A_{\text{T}}$ , as detailed in the OCMIP2 design document (Najjar and Orr, 1998) and in the OCMIP2 Abiotic HOWTO (Orr et al., 1999b). In OMIP, all models should report air–sea  $\text{CO}_2$  fluxes due to gas exchange ( $F_{\text{CO}_2}$ ,  $F_{\text{CO}_2}^{\text{nat}}$ ,  $F_{\text{CO}_2}^{\text{abio}}$ ,  $F_{^{14}\text{CO}_2}^{\text{abio}}$ , and  $F_{^{13}\text{CO}_2}$ ) without virtual fluxes included. Virtual fluxes are not requested as they do not directly represent  $\text{CO}_2$  exchange between the atmosphere and ocean.

Surface boundary fluxes may be coded simply as adding source–sink terms to the surface layer, e.g.,

$$J_A = \frac{F_A}{\Delta z_1}, \quad (5)$$

where for gas  $A$ ,  $J_A$  is its surface-layer source–sink term due to gas exchange ( $\text{mol m}^{-3} \text{ s}^{-1}$ ) and  $F_A$  is its air-to-sea flux ( $\text{mol m}^{-2} \text{ s}^{-1}$ ), while  $\Delta z_1$  is the surface-layer thickness (m).

In OMIP, we parameterize air–sea gas transfer of CFC-11, CFC-12,  $\text{SF}_6$ ,  $\text{O}_2$ ,  $\text{CO}_2$ ,  $^{14}\text{CO}_2$ , and  $^{13}\text{CO}_2$  using the gas transfer formulation also adopted for OCMIP2 (excluding effects of bubbles):

$$F_A = k_w ([A]_{\text{sat}} - [A]), \quad (6)$$

where for gas  $A$ ,  $k_w$  is its gas transfer velocity,  $[A]$  is its simulated surface-ocean dissolved concentration, and  $[A]_{\text{sat}}$  is its corresponding saturation concentration in equilibrium with the water-vapor-saturated atmosphere at a total atmospheric pressure  $P_{\text{a}}$ . Concentrations throughout are indicated by square brackets and are in units of  $\text{mol m}^{-3}$ .

For all gases that remain purely in dissolved form in seawater, gas exchange is modeled directly with Eq. (6). However, for  $C_{\text{T}}$ , only a small part remains as dissolved gas as mentioned in Sect. 2.6. Thus the dissolved gas concentration  $[\text{CO}_2^*]$  must first be computed, each time step, from modeled  $C_{\text{T}}$  and  $A_{\text{T}}$ , and then the gas exchange is computed with Eq. (6). For example, for the two abiotic tracers (in *omip1-spinup*),

$$F_{\text{CO}_2^{\text{abio}}} = k_w ([\text{CO}_2^*]_{\text{sat}} - [\text{CO}_2^*]) \quad (7)$$

and

$$F_{^{14}\text{CO}_2^{\text{abio}}} = k_w ([^{14}\text{CO}_2^*]_{\text{sat}} - [^{14}\text{CO}_2^*]). \quad (8)$$

For  $^{13}\text{C}$ , isotopic fractionation associated with gas exchange must be included in the flux calculation. We recom-

mend using the formulation of Zhang et al. (1995):

$$F_{13\text{CO}_2} = k_w \alpha_k \alpha_{\text{aq-g}} \left( {}^{13}R_{\text{atm}} [\text{CO}_2^*]_{\text{sat}} - \frac{[{}^{13}\text{CO}_2^*]}{\alpha_{\text{C-T-g}}} \right), \quad (9)$$

where  $\alpha_k$  is the kinetic fractionation factor,  $\alpha_{\text{aq-g}}$  is the fractionation factor for gas dissolution,  $\alpha_{\text{C-T-g}}$  is the equilibrium fractionation factor between dissolved inorganic carbon and gaseous  $\text{CO}_2$ , and  ${}^{13}R_{\text{atm}}$  is the  ${}^{13}\text{C}/{}^{12}\text{C}$  ratio in atmospheric  $\text{CO}_2$ . Following Zhang et al. (1995),  $\alpha_{\text{C-T-g}}$  depends on  $T$  and the fraction of carbonate in  $\text{C}_\text{T}$ , namely  $f\text{CO}_3$ :

$$\alpha_{\text{C-T-g}} = \frac{0.0144 T_c f\text{CO}_3 - 0.107 T_c + 10.53}{1000} + 1, \quad (10)$$

where  $T_c$  is temperature in units of  $^\circ\text{C}$ , while division by 1000 and addition of 1 converts the fractionation factor from  $\epsilon$  in units of ‰ into  $\alpha$ . The  $\alpha_{\text{aq-g}}$  term depends on temperature following

$$\alpha_{\text{aq-g}} = \frac{0.0049 T_c - 1.31}{1000} + 1. \quad (11)$$

Conversely no temperature dependence was found for  $\alpha_k$ . Hence we recommend that OMIP modelers use a constant value for  $\alpha_k$  of 0.99912 ( $\epsilon_k$  of  $-0.88$  ‰), the average from the Zhang et al. (1995) measurements at 5 and  $21$   $^\circ\text{C}$ .

### 2.5.1 Gas transfer velocity

OMIP modelers should use the instantaneous gas transfer velocity  $k_w$  parameterization from Wanninkhof (1992), a quadratic function of the 10 m wind speed  $u$

$$k_w = a \left( \frac{Sc}{660} \right)^{-1/2} u^2 (1 - f_i), \quad (12)$$

to which we have added limitation from sea-ice cover following OCMIP2. Here  $a$  is a constant,  $Sc$  is the Schmidt number, and  $f_i$  is the sea-ice fractional coverage of each grid cell (varying from 0 to 1). Normally, the constant  $a$  is adjusted so that wind speeds used to force the model are consistent with the observed global inventory of bomb  ${}^{14}\text{C}$ , e.g., as done in previous phases of OCMIP (Orr et al., 2001; Najjar et al., 2007). Here though, we choose to use one value of  $a$  for all simulations, independent of whether models are used in forced (OMIP) or coupled mode, namely the CMIP6 DECK (Diagnostic, Evaluation and Characterization of Klima) and historical simulations. For  $a$  in OMIP, we rely on the reassessment from Wanninkhof (2014), who used improved estimates of the global-ocean bomb- ${}^{14}\text{C}$  inventory along with CCMP (Cross Calibrated Multi-Platform) wind fields in an inverse approach with the Modular Ocean Model (Sweeney et al., 2007) to derive a best value of

$$a = 0.251 \frac{\text{cm h}^{-1}}{(\text{m s}^{-1})^2}, \quad (13)$$

which will give  $k_w$  in  $\text{cm h}^{-1}$  if winds speeds are in  $\text{m s}^{-1}$ . For model simulations where tracers are carried in  $\text{mol m}^{-3}$ ,  $k_w$  should be in units of  $\text{m s}^{-1}$ ; thus,  $a$  should be set equal to  $6.97 \times 10^{-7} \text{ m s}^{-1}$ . The same value of  $a$  should be adopted for the forced OMIP simulations and for ESM simulations made under CMIP6.

### 2.5.2 Schmidt number

Besides  $a$ , the Schmidt number  $Sc$  is also needed to compute the gas transfer velocity (Eq. 12). The Schmidt number is the ratio of the kinematic viscosity of water  $\nu$  to the diffusion coefficient of the gas  $D$  ( $Sc = \nu/D$ ). The coefficients for the fourth-order polynomial fit of  $Sc$  to in situ temperature over the temperature range of  $-2$  to  $40$   $^\circ\text{C}$  (Wanninkhof, 2014) are provided in Table 1 for each gas to be modeled in OMIP and CMIP6. Fortran 95 routines using the same formula and coefficients for all gases modeled in OMIP are available for download via the *gasx* module of the *mocsy* package (Sect. 2.6).

### 2.5.3 Atmospheric saturation concentration

The surface gas concentration in equilibrium with the atmosphere (saturation concentration) is

$$\begin{aligned} [A]_{\text{sat}} &= K_0 f_A = K_0 C_f p_A \\ &= K_0 C_f (P_a - p\text{H}_2\text{O}) x_A, \end{aligned} \quad (14)$$

where for gas  $A$ ,  $K_0$  is its solubility,  $f_A$  is its atmospheric fugacity,  $C_f$  is its fugacity coefficient,  $p_A$  is its atmospheric partial pressure, and  $x_A$  is its mole fraction in dry air, while  $P_a$  is again the total atmospheric pressure (atm) and  $p\text{H}_2\text{O}$  is the vapor pressure of water (also in atm) at sea surface temperature and salinity (Weiss and Price, 1980).

The combined term  $K_0 C_f (P_a - p\text{H}_2\text{O})$  is available at  $P_a = 1$  atm (i.e.,  $P_a^0$ ) for all modeled gases except oxygen. We denote this combined term as  $\phi_A^0$  (at  $P_a^0$ ); elsewhere it is known as the solubility function  $F$  (e.g., Weiss and Price, 1980; Warner and Weiss, 1985; Bullister et al., 2002), but we do not use the latter notation here to avoid confusion with the air–sea flux (Eq. 6). For four of the gases to be modeled in OMIP, the combined solubility function  $\phi_A^0$  has been computed using the empirical fit

$$\begin{aligned} \ln(\phi_A^0) &= a_1 + a_2 \left( \frac{100}{T} \right) + a_3 \ln \left( \frac{T}{100} \right) + a_4 \left( \frac{T}{100} \right)^2 \\ &\quad + S \left[ b_1 + b_2 \left( \frac{T}{100} \right) + b_3 \left( \frac{T}{100} \right)^2 \right], \end{aligned} \quad (15)$$

where  $T$  is the model's in situ, absolute temperature (ITS90) and  $S$  is its salinity on the practical salinity scale (PSS-78). Thus separate sets of coefficients are available for  $\text{CO}_2$  (Weiss and Price, 1980, Table VI), CFC-11 and CFC-12 (Warner and Weiss, 1985, Table 5), and  $\text{SF}_6$  (Bullister et al.,

**Table 1.** Seawater coefficients for fit of  $S_c$  to temperature<sup>a,b</sup> from Wanninkhof (2014).

Gas	$A$	$B$	$C$	$D$	$E$	$S_c$ (20 °C)
CFC-11	3579.2	−222.63	7.5749	−0.14595	0.0011874	1179
CFC-12	3828.1	−249.86	8.7603	−0.1716	0.001408	1188
SF <sub>6</sub>	3177.5	−200.57	6.8865	−0.13335	0.0010877	1028
CO <sub>2</sub>	2116.8	−136.25	4.7353	−0.092307	0.0007555	668
O <sub>2</sub>	1920.4	−135.6	5.2122	−0.10939	0.00093777	568
N <sub>2</sub> O	2356.2	−166.38	6.3952	−0.13422	0.0011506	697
DMS	2855.7	−177.63	6.0438	−0.11645	0.00094743	941

<sup>a</sup> Coefficients for fit to  $S_c = A + BT_c + CT_c^2 + DT_c^3 + ET_c^4$ , where  $T_c$  is surface temperature in °C.

<sup>b</sup> Conservative temperature should be converted to in situ temperature before using these coefficients.

**Table 2.** Coefficients for fit<sup>a,b,c</sup> of solubility function  $\phi_A^0$  (mol L<sup>−1</sup> atm<sup>−1</sup>).

Gas	$a_1$	$a_2$	$a_3$	$a_4$	$b_1$	$b_2$	$b_3$
CFC-11	−229.9261	319.6552	119.4471	−1.39165	−0.142382	0.091459	−0.0157274
CFC-12	−218.0971	298.9702	113.8049	−1.39165	−0.143566	0.091015	−0.0153924
SF <sub>6</sub>	−80.0343	117.232	29.5817	0.0	0.0335183	−0.0373942	0.00774862
CO <sub>2</sub>	−160.7333	215.4152	89.8920	−1.47759	0.029941	−0.027455	0.0053407
N <sub>2</sub> O	−165.8806	222.8743	92.0792	−1.48425	−0.056235	0.031619	−0.0048472

<sup>a</sup> Fit to Eq. (15), where  $T$  is in situ, absolute temperature (K) and  $S$  is salinity (practical salinity scale). <sup>b</sup> For units of mol m<sup>−3</sup> atm<sup>−1</sup>, coefficients should be multiplied by 1000. <sup>c</sup> The units refer to atm of each gas, not atm of air. <sup>d</sup> When using these coefficients, conservative temperature should be converted to in situ temperature (K) and absolute salinity should be converted to practical salinity.

2002, Table 3), the values of which are summarized here in Table 2. For O<sub>2</sub>, it is not  $\phi_A^0$  that is available, but rather  $[O_2]_{\text{sat}}^0$  (Garcia and Gordon, 1992), as detailed below.

Both the solubility function  $\phi_A^0$  and the saturation concentration  $[A]_{\text{sat}}^0$  can be used at any atmospheric pressure  $P_a$ , with errors of less than 0.1 %, by approximating Eq. (14) as

$$[A]_{\text{sat}} = \frac{P_a}{P_a^0} \phi_A^0 x_A = \frac{P_a}{P_a^0} [A]_{\text{sat}}^0, \quad (16)$$

where  $P_a^0$  is the reference atmospheric pressure (1 atm). Variations in surface atmospheric pressure must not be neglected in OMIP because they alter the regional distribution of  $[A]_{\text{sat}}$ . For example, the average surface atmospheric pressure between 60 and 30° S is 3 % lower than the global mean, thus reducing surface-ocean  $p\text{CO}_2$  by 10  $\mu\text{atm}$  and  $[O_2]_{\text{sat}}$  by 10  $\mu\text{mol kg}^{-1}$ . The atmospheric pressure fields used to compute gas saturations should also be consistent with the other physical forcing. Thus for the OMIP forced simulations, modelers will use surface atmospheric pressure from CORE II, converted to atm.

For the two abiotic carbon tracers, abbreviating  $K' = K_0 C_f$ , we can write their surface saturation concentrations (Eq. 14) as

$$[\text{CO}_2^*]_{\text{sat}}^{\text{abio}} = K' (P_a - p\text{H}_2\text{O}) x_{\text{CO}_2} \quad (17)$$

and

$$[^{14}\text{CO}_2^*]_{\text{sat}}^{\text{abio}} = [\text{CO}_2^*]_{\text{sat}}^{\text{abio}} {}^{14}r'_{\text{atm}}. \quad (18)$$

Here  ${}^{14}r'_{\text{atm}}$  represents the normalized atmospheric ratio of  ${}^{14}\text{C}/\text{C}$ , i.e.,

$${}^{14}r'_{\text{atm}} = \frac{{}^{14}r_{\text{atm}}}{{}^{14}r_{\text{std}}} = \left(1 + \frac{\Delta^{14}\text{C}_{\text{atm}}}{1000}\right), \quad (19)$$

where  ${}^{14}r_{\text{atm}}$  is the atmospheric ratio of  ${}^{14}\text{C}/\text{C}$ ,  ${}^{14}r_{\text{std}}$  is the analogous ratio for the standard ( $1.170 \times 10^{-12}$ ; see Appendix A), and  $\Delta^{14}\text{C}_{\text{atm}}$  is the atmospheric  $\Delta^{14}\text{C}$ , the fractionation-corrected ratio of  ${}^{14}\text{C}/\text{C}$  relative to a standard reference given in permil (see below). We define  ${}^{14}r'_{\text{atm}}$  and use it in Eq. (18) to be able to compare  ${}^{14}C_{\text{T}}^{\text{abio}}$  and  $C_{\text{T}}^{\text{abio}}$  directly, potentially simplifying code verification and testing. With the above model formulation for the OMIP equilibrium run (where  $x\text{CO}_2^{\text{atm}} = 284.32$  ppm and  $\Delta^{14}\text{C}^{\text{atm}} = 0\text{‰}$ ), both  $C_{\text{T}}^{\text{abio}}$  and  ${}^{14}C_{\text{T}}^{\text{abio}}$  have identical units. Short tests with the same initialization for both tracers can thus verify consistency. Differences in the spin-up simulation will stem only from different initializations and radioactive decay. Differences will grow further during the anthropogenic perturbation (in *omip1-spinup*, i.e., after spin-up) because of the sharp contrast between the shape of the atmospheric histories of  $x\text{CO}_2$  and  $\Delta^{14}\text{C}_{\text{atm}}$ .

For  ${}^{13}\text{C}$ , the  $\delta^{13}\text{C}_{\text{atm}}$  in atmospheric CO<sub>2</sub> is incorporated into Eq. (9) through the term  ${}^{13}R_{\text{atm}}$ , which is given by

$${}^{13}R_{\text{atm}} = \left(\frac{\delta^{13}\text{C}_{\text{atm}}}{1000} + 1\right) {}^{13}R_{\text{std}}, \quad (20)$$

**Table 3.** Coefficients for fit of  $K'$  and  $K_0$  (both in  $\text{mol L}^{-1} \text{atm}^{-1}$ ).

Gas	$a_1$	$a_2$	$a_3$	$b_1$	$b_2$	$b_3$
$K'$						
CFC-11	−134.1536	203.2156	56.2320	−0.144449	0.092952	−0.0159977
CFC-12	−122.3246	182.5306	50.5898	−0.145633	0.092509	−0.0156627
SF <sub>6</sub>	−96.5975	139.883	37.8193	0.0310693	−0.0356385	0.00743254
$K_0$						
CO <sub>2</sub>	−58.0931	90.5069	22.2940	0.027766	−0.025888	0.0050578
N <sub>2</sub> O	−62.7062	97.3066	24.1406	−0.058420	0.033193	−0.0051313

<sup>a</sup> Fit to Eq. (24), where  $T$  is in situ, absolute temperature (K) and  $S$  is practical salinity. <sup>b</sup> The final three footnotes of Table 2 also apply here.

where  $^{13}R_{\text{std}}$  is the standard ratio 0.0112372 (Craig, 1957). In this formulation, unlike for  $^{14}C_{\text{T}}^{\text{abio}}$ ,  $^{13}C_{\text{T}}$  is not normalized by the standard ratio. However, modeling groups may wish to simulate normalized  $^{13}C_{\text{T}}$ , e.g., by including a factor of  $1/^{13}R_{\text{std}}$  analogous to the approach used for  $^{14}C_{\text{T}}^{\text{abio}}$ . Modeling groups that simulate  $^{13}C$  in OMIP must report non-normalized values of the concentration  $^{13}C_{\text{T}}$  and the air–sea flux  $F_{^{13}\text{CO}_2}$ . No other  $^{13}C$  results are requested.

For all gases simulated in OMIP, the atmospheric saturation concentration  $[A]_{\text{sat}}$  is computed using Eq. (16). For all gases except oxygen, the combined solubility function  $\phi_{\text{A}}^0$  is available, being computed each time step using modeled  $T$  and  $S$  with Eq. (15), the corresponding gas-specific coefficients (Table 2), and the atmospheric mole fraction of each gas  $x_{\text{A}}$ . The exception is O<sub>2</sub> because rather than  $x_{\text{A}}$  and  $\phi_{\text{A}}^0$ , it is the reference saturation concentration  $[O_2]_{\text{sat}}^0$  that is available (Garcia and Gordon, 1992, Eq. 8, Table 1).

In all cases, the same  $P_{\text{a}}/P_{\text{a}}^0$  term is used to account for effects of atmospheric pressure (Eq. 16). For  $P_{\text{a}}$ , modelers must use the fields of surface atmospheric pressure (*sap*) from CORE II, i.e., for OMIP's forced ocean simulations (*omip1* and *omip1-spinup*), whereas for any CMIP6 coupled simulation, modelers should use *sap* from the coupled atmospheric model.

To compute  $[A]_{\text{sat}}$  then, we only need one additional type of information, namely the  $x_{\text{A}}$ 's for each of CO<sub>2</sub>, CFC-11, CFC-12, and SF<sub>6</sub>, as well as corresponding atmospheric histories for carbon isotopes.

1.  $x_{\text{CFC-11}}$ ,  $x_{\text{CFC-12}}$ , and  $x_{\text{SF}_6}$ . Atmospheric records for observed CFC-11 and CFC-12 (in parts per trillion – ppt) are based on station data at 41° S and 45° N from Walker et al. (2000) with subsequent extensions as compiled by Bullister (2015). For OMIP, each station will be treated as representative of its own hemisphere, except between 10° S and 10° N, where those station values will be interpolated linearly as a function of latitude. Thus there are three zones: 90–10° S, where CFCs are held to the same value as at the station at 41° S; 10° S–10° N, a buffer zone where values

are interpolated linearly; and 10–90° N, where values are held to the same value as at the measuring station at 45° N. For SF<sub>6</sub>, OMIP also relies on the Bullister (2015) synthesis over the same latitudinal bands. Values for all three inert chemical tracers are given at mid-year. It is recommended that modelers linearly interpolate these mid-year values to each time step, because annual growth rates can be large and variable. These atmospheric records are available at [http://cdiac.ornl.gov/ftp/oceans/CFC\\_ATM\\_Hist/CFC\\_ATM\\_Hist\\_2015](http://cdiac.ornl.gov/ftp/oceans/CFC_ATM_Hist/CFC_ATM_Hist_2015); eventually they will be made available at input4mips (<https://esgf-node.llnl.gov/search/input4mips>).

2.  $x_{\text{CO}_2}$ . In the *spin-up* simulation, needed to initialize *omip1-spinup* simulation, atmospheric CO<sub>2</sub> is held constant at  $x_{\text{CO}_2} = 284.32$  ppm, the same preindustrial value as used for the CMIP6 *piControl* simulation. Over the industrial era, defined as between years 1850.0 and 2010.0 for both of OMIP's transient simulations (*omip1* and *omip1-spinup*), atmospheric  $x_{\text{CO}_2}$  will follow the same observed historical increase as provided for CMIP6 (Meinshausen et al., 2016). Modelers should use the record of global annual-mean atmospheric  $x_{\text{CO}_2}$ , interpolated to each time step. That increasing  $x_{\text{CO}_2}$  affects the total tracer  $C_{\text{T}}$  in both transient simulations as well as the two abiotic tracers and  $^{13}C_{\text{T}}$  in the *omip1-spinup* simulation. However, it does not affect the natural tracer  $C_{\text{T}}^{\text{nat}}$ , for which the atmosphere is always held at  $x_{\text{CO}_2} = 284.32$  ppm. These  $x_{\text{CO}_2}$  data are available in the supplement to (Meinshausen et al., 2016).
3.  $\Delta^{14}C^{\text{atm}}$ . For the OMIP spin-up simulation,  $\Delta^{14}C^{\text{atm}}$  is held constant at 0‰. For the *omip1-spinup* simulation, the equilibrium reference is thus year 1850.0. Then the model must be integrated until 2010.0 following the observed record of  $\Delta^{14}C^{\text{atm}}$ , separated into three latitudinal bands (90–20° S, 20° S–20° N, and 20–90° N). The  $\Delta^{14}C^{\text{atm}}$  record is the same as adopted for C4MIP, a compilation of tree-ring and atmospheric measurements from (Levin et al., 2010) and other

sources (I. Levin, personal communication, 2016). It is available at input4mips (<https://esgf-node.llnl.gov/search/input4mips>).

4.  $\delta^{13}\text{C}^{\text{atm}}$ . The atmospheric record of  $\delta^{13}\text{C}$  is the same as adopted for C4MIP, a compilation of ice-core data (Rubino et al., 2013) and atmospheric measurements at Mauna Loa (Keeling et al., 2001). It is available at input4mips (<https://esgf-node.llnl.gov/search/input4mips>).

## 2.5.4 Surface-ocean concentration

The equation above for the atmospheric equilibrium (saturation) concentration of a gas (Eq. 14) should not be confused with the analogous equation for the simulated ocean concentration. The surface-ocean equation allows conversion between the simulated surface-ocean dissolved gas concentration  $[A]$ , the corresponding fugacity  $f_{\text{O}}$ , and the partial pressure  $p_{\text{O}}$  of the surface ocean as follows:

$$[A] = K_0 f_{\text{O}} = K_0 C_{\text{f}} p_{\text{O}} = K' p_{\text{O}}. \quad (21)$$

This surface-ocean equation is analogous to that for the atmospheric equilibrium saturation concentration  $[A]_{\text{sat}}$  (Eq. 14), except that the ocean equation omits the final portion of the atmospheric equation which computes the mole fraction, a conventional parameter only for the atmosphere. Thus the combined term that includes the atmospheric pressure and humidity corrections (last term in parentheses) in Eq. (14) is not pertinent for the surface-ocean equation. It should not be used when converting between simulated oceanic  $[A]$  and the corresponding  $p_{\text{O}}$ . Confusion on this point was apparent in the publicly available OMIP2 code, i.e., for the conversion from  $[\text{CO}_2^*]$  to  $p\text{CO}_2$ , although that did not affect simulated  $F_{\text{CO}_2}$ .

To avoid potential confusion and redundancy, OMIP modelers may prefer to separately compute the parts of  $\phi_{\text{A}}$  rather than computing  $\phi_{\text{A}}^0$  and using it directly. Since

$$\phi_{\text{A}} = K_0 C_{\text{f}} (P_{\text{a}} - p_{\text{H}_2\text{O}}) = K' (P_{\text{a}} - p_{\text{H}_2\text{O}}), \quad (22)$$

modelers need only compute  $K'$ , and use that in both the ocean equation (Eq. 21) and the atmospheric saturation equation (Eq. 14), while for the latter also correct for atmospheric pressure and humidity, i.e., the  $(P_{\text{a}} - p_{\text{H}_2\text{O}})$  term. That combined correction is to be computed with  $P_{\text{a}}$  from the CORE II forcing and with  $p_{\text{H}_2\text{O}}$  calculated from model surface  $T$  and  $S$  (Weiss and Price, 1980, Eq. 10):

$$p_{\text{H}_2\text{O}} = 24.4543 - 67.4509 \left( \frac{100}{T} \right) - 4.8489 \ln \left( \frac{T}{100} \right) - 0.000544 S, \quad (23)$$

where  $p_{\text{H}_2\text{O}}$  is in atm,  $T$  is the in situ, absolute temperature, and  $S$  is practical salinity. In this way, OMIP modelers

may avoid using the sometimes confusing combined term  $\phi_{\text{A}}^0$  altogether as well as its approximative pressure correction when calculating the saturation concentration (Eq. 16). Pressure corrections for  $K'$  may be neglected in the surface ocean where total pressure remains close to 1 atm (Weiss, 1974).

The ocean equation (Eq. 21) converts a simulated dissolved gas concentration to a partial pressure using its combined product  $K'$ , which can be computed directly for some gases or via a two-step process for others. For OMIP's inert chemical tracers, tabulated coefficients can be used to compute  $K'$  directly, i.e., for CFC-11 and CFC-12 (Warner and Weiss, 1985, Table 2) and for SF<sub>6</sub> (Bullister et al., 2002, Table 2) using modeled  $T$  and  $S$  in an equation just like Eq. (15) but without the first  $T^2$  term ( $a_4 = 0$ ):

$$\ln(K') = a_1 + a_2 \left( \frac{100}{T} \right) + a_3 \ln \left( \frac{T}{100} \right) + S \left[ b_1 + b_2 \left( \frac{T}{100} \right) + b_3 \left( \frac{T}{100} \right)^2 \right], \quad (24)$$

where  $T$  is the in situ absolute temperature and  $S$  is practical salinity.

For O<sub>2</sub>,  $K'$  is not needed for the saturation calculations, but it is necessary when using the simulated dissolved  $[\text{O}_2]$  to compute the corresponding surface-ocean  $p\text{O}_2$ , an output variable for OMIP and CMIP6. That solubility conversion factor  $K'$  can be derived by substituting its definition into Eq. (14) and rearranging, so that

$$K'_{\text{O}_2} = \frac{[\text{O}_2]_{\text{sat}}^0}{x_{\text{O}_2} (P_{\text{a}}^0 - p_{\text{H}_2\text{O}})}, \quad (25)$$

where the numerator is from Eq. (8) of Garcia and Gordon (1992) using coefficients from their Table 1, and the denominator is the product of the corresponding constant atmospheric mole fraction of O<sub>2</sub> ( $x_{\text{O}_2} = 0.20946$ ) and the wet-to-dry correction at 1 atm as described above. The computed  $K'_{\text{O}_2}$  is then exploited to compute the partial pressure of oxygen ( $p\text{O}_2 = [\text{O}_2]/K'_{\text{O}_2}$ ).

For CO<sub>2</sub>, tabulated coefficients are not available to compute  $K'$ , but they are available to compute  $K_0$  (Weiss, 1974, Table 1). Hence given that  $K' = K_0 C_{\text{f}}$ , modelers must also compute the fugacity coefficient  $C_{\text{f}}$  from Eq. (9) of Weiss (1974):

$$C_{\text{f}} = \exp \left[ \left( B + 2x_2^2 \delta_{12} \right) \frac{P_{\text{ao}}}{RT} \right], \quad (26)$$

where  $B$  is the virial coefficient of CO<sub>2</sub> (Weiss, 1974, Eq. 6),  $x_2$  is the sum of the mole fractions of all remaining gases ( $1 - x_{\text{CO}_2}$ , when  $x_{\text{CO}_2} \ll 1$ ), and  $\delta_{12} = 57.7 - 0.118 T$ . Here  $P_{\text{ao}}$  is the total pressure (atmospheric + hydrostatic) in atm,  $R$  is the gas constant ( $82.05736 \text{ cm}^3 \text{ atm mol}^{-1} \text{ K}^{-1}$ ), and  $T$  is the in situ absolute temperature (K).

Although the surface-ocean concentration of dissolved carbon dioxide gas  $[\text{CO}_2^*]$  is needed to compute air–sea CO<sub>2</sub>

exchange, it is not that inorganic carbon species that is carried as a tracer in ocean carbon models (Sect. 2.6). Instead the  $[\text{CO}_2^*]$  concentration ( $\text{mol m}^{-3}$ ) must be computed each time step from a model's simulated surface  $C_T$ ,  $A_T$ ,  $T$ , and  $S$  as well as nutrient concentrations (total dissolved inorganic phosphorus  $P_T$  and silicon  $Si_T$ ) as detailed in the following section. All OMIP biogeochemical models will carry  $C_T$  and  $A_T$  as passive tracers. Most if not all models will also carry at least one inorganic nutrient, nitrogen or phosphorus. Some will carry silicon. For models that carry only nitrogen, it is preferred that they compute and report  $P_T$  by dividing the total dissolved inorganic nitrogen concentration by 16, the constant N:P ratio from Redfield et al. (1963). For models without  $Si_T$ , it is preferred that they use climatological  $Si_T$  data interpolated to their model grid (i.e., annual average data from WOA2013). These options offer a better alternative than assuming that nutrient concentrations are zero, which leads to systematic shifts on the order of  $10 \mu\text{atm}$  in calculated surface-water  $p\text{CO}_2$ .

The abiotic portion of the biogeochemical simulation carries only two tracers,  $C_T^{\text{abio}}$  and  $^{14}C_T^{\text{abio}}$ , which are not connected to other biogeochemical tracers. Hence to compute corresponding abiotic  $[\text{CO}_2^*]$  and  $^{14}\text{CO}_2^*$  concentrations, we also need abiotic alkalinity. Following OCMIP2, the abiotic alkalinity in OMIP will be calculated simply as a normalized linear function of salinity:

$$A_T^{\text{abio}} = \bar{A}_T \left( \frac{S}{\bar{S}} \right), \quad (27)$$

where  $\bar{A}_T$  is the global mean of surface observations  $2297 \mu\text{mol kg}^{-1}$  (Lauvset et al., 2016) and  $\bar{S}$  is the model's global- and annual-mean surface salinity. In practice, it is recommended that  $\bar{S}$  is first computed as the global mean of the initial salinity field and then, after 1 year of simulation, from the annual-mean salinity of the previous year. Also needed are two other input arguments,  $P_T$  and  $Si_T$ . Although accounting for both of their acid systems makes a difference, these abiotic tracers are not included along with abiotic  $C_T$ . Hence we take their concentrations as being constant, equal to the global mean of surface observations for  $P_T$  of  $0.5 \mu\text{mol kg}^{-1}$  and for  $Si_T$  of  $7.5 \mu\text{mol kg}^{-1}$ . The assumption of constant nutrient distributions applies only to the carbonate chemistry calculations for abiotic  $C_T$  (i.e.,  $C_T^{\text{abio}}$ ).

For the abiotic simulation's radiocarbon tracer, we must likewise compute its surface-ocean dissolved gas concentration  $^{14}\text{CO}_2^*$ . The latter is related to the calculated dissolved gas concentration of the stable abiotic carbon tracer as follows:

$$^{14}\text{CO}_2^*]^{\text{abio}} = [\text{CO}_2^*]^{\text{abio}} {}^{14}r'_{\text{ocn}}, \quad (28)$$

where

$${}^{14}r'_{\text{ocn}} = \frac{{}^{14}r_{\text{ocn}}}{{}^{14}r_{\text{std}}} = \frac{{}^{14}C_T^{\text{abio}}}{C_T^{\text{abio}}} \quad (29)$$

and  ${}^{14}r_{\text{ocn}}$  is the  $^{14}\text{C}/\text{C}$  of seawater. This normalization essentially means that  $^{14}C_T^{\text{abio}}$  represents the actual fractionation-corrected  $^{14}\text{C}$  concentration divided by  ${}^{14}r_{\text{std}}$ . This output must be saved in normalized form. But for subsequent  $^{14}\text{C}$  budget calculations, it will be necessary to back-correct the normalized and fractionation-corrected modeled concentration ( $^{14}C_T^{\text{abio}}$ ) and  $^{14}\text{C}$  flux ( $F_{^{14}\text{CO}_2^{\text{abio}}}$ ), i.e., the only two  $^{14}\text{C}$  variables saved in OMIP, to molar units of actual  $^{14}\text{C}$  (see Appendix A). For eventual comparison to ocean measurements, one can compute oceanic  $\Delta^{14}\text{C}$  as

$$\Delta^{14}C_{\text{ocn}}^{\text{abio}} = 1000 \left( {}^{14}r'_{\text{ocn}} - 1 \right). \quad (30)$$

For  $^{13}\text{C}$ , the surface-ocean dissolved gas concentration  $^{13}\text{CO}_2^*$  is given by

$$^{13}\text{CO}_2^* = [\text{CO}_2^*] {}^{13}r_{\text{ocn}}, \quad (31)$$

where  ${}^{13}r_{\text{ocn}} = {}^{13}C_T/C_T$ . Here  ${}^{13}C_T$  is not normalized by the standard ratio, but modeling groups may wish to simulate normalized  ${}^{13}C_T$  by including a factor of  $1/{}^{13}r_{\text{std}}$ , analogous to what is done for the  $^{14}C_T^{\text{abio}}$  normalization above.

## 2.6 Carbonate chemistry

Unlike other modeled gases in OMIP,  $\text{CO}_2$  does not occur in seawater as a simple dissolved passive tracer. Instead, it reacts with seawater, forming carbonic acid ( $\text{H}_2\text{CO}_3$ ), most of which dissociates into two other inorganic species, bicarbonate ( $\text{HCO}_3^-$ ) and carbonate ( $\text{CO}_3^{2-}$ ) ions. Since dissolved  $\text{CO}_2$  cannot be distinguished analytically from the much less abundant  $\text{H}_2\text{CO}_3$ , common practice is to refer to the sum of the two,  $\text{CO}_2 + \text{H}_2\text{CO}_3$ , as  $\text{CO}_2^*$ . The sum of the three species  $\text{CO}_2^* + \text{HCO}_3^- + \text{CO}_3^{2-}$  is referred to as total dissolved inorganic carbon  $C_T$ , while their partitioning depends on seawater pH, temperature, salinity, and pressure. The pH may be calculated from  $C_T$  and seawater's ionic charge balance, formalized as total alkalinity  $A_T$ . Both  $C_T$  and  $A_T$  are conservative with respect to mixing and changes in seawater temperature, salinity, and pressure. Hence both are carried as passive tracers in all ocean models, and both are used, along with temperature, salinity, and nutrient concentrations, to compute the dissolved concentration of  $\text{CO}_2$  and the related  $p\text{CO}_2$ , as needed to compute air–sea  $\text{CO}_2$  fluxes.

To simulate carbonate chemistry, OMIP groups should use the total pH scale and the equilibrium constants recommended for best practices (Dickson et al., 2007; Dickson, 2010). Additionally, the model's total alkalinity equation should include alkalinity from phosphoric and silicic acid systems as well as from carbonic acid, boric acid, and water, namely

$$A_T = A_C + A_B + A_W + A_P + A_{Si} + A_O, \quad (32)$$

**Table 4.** Output for inert chemistry.

Symbol	Variable name	Units	Shape	Priority	Long name
Annual means					
SF <sub>6</sub>	sf6	mol m <sup>-3</sup>	XYZ	2	Mole concentration of SF6 in seawater
CFC-11	cfc11	mol m <sup>-3</sup>	XYZ	2	Mole concentration of CFC-11 in seawater
CFC-12	cfc12	mol m <sup>-3</sup>	XYZ	1	Mole concentration of CFC-12 in seawater
Monthly means					
SF <sub>6</sub>	sf6	mol m <sup>-3</sup>	XYZ	2	Mole concentration of SF6 in seawater
CFC-11	cfc11	mol m <sup>-3</sup>	XYZ	2	Mole concentration of CFC-11 in seawater
CFC-12	cfc12	mol m <sup>-3</sup>	XYZ	1	Mole concentration of CFC-12 in seawater
<i>F</i> <sub>SF<sub>6</sub></sub>	fgsf6	mol m <sup>-2</sup> s <sup>-1</sup>	XY	2	Surface downward SF6 flux
<i>F</i> <sub>CFC-11</sub>	fgcfc11	mol m <sup>-2</sup> s <sup>-1</sup>	XY	2	Surface downward CFC-11 flux
<i>F</i> <sub>CFC-12</sub>	fgcfc12	mol m <sup>-2</sup> s <sup>-1</sup>	XY	1	Surface downward CFC-12 flux

**Table 5.** Daily mean biogeochemical output.

Variable name	Units	Shape	Priority	Long name
chlos	kg m <sup>-3</sup>	XY	3	Surface mass conc. of total phytoplankton expressed as chlorophyll seawater
phycos	mol m <sup>-3</sup>	XY	3	Surface phytoplankton carbon concentration

where

$$A_C = [\text{HCO}_3^-] + 2[\text{CO}_3^{2-}], \quad (33)$$

$$A_B = [\text{B(OH)}_4^-], \quad (34)$$

$$A_W = [\text{OH}^-] - [\text{H}^+]_F - [\text{HSO}_4^-] - [\text{HF}], \quad (35)$$

$$A_P = [\text{HPO}_4^{2-}] + 2[\text{PO}_4^{3-}] - [\text{H}_3\text{PO}_4], \quad (36)$$

$$A_{\text{Si}} = [\text{SiO(OH)}_3^-], \quad (37)$$

$$A_O = [\text{NH}_3] + [\text{HS}^-] + \dots \quad (38)$$

The right side of Eq. (32) thus separates the contributions from components of carbonic acid, boric acid, water, phosphoric acid, silicic acid, and other species, respectively. Neglect of  $A_P$  and  $A_{\text{Si}}$  has been common among model groups but leads to systematic errors in computed  $p\text{CO}_2$ , e.g., in the Southern Ocean (Najjar and Orr, 1998; Orr et al., 2015). Models with the nitrogen cycle should also account for effects of changes in the different inorganic forms of nitrogen on total alkalinity, including changes due to denitrification and nitrogen fixation plus nitrification. Models with  $P_T$  as the sole macronutrient tracer should consider accounting for the effect of nitrate assimilation and remineralization on alkalinity, effects that are 16 times larger than for those for  $P_T$  (Wolf-Gladrow et al., 2007).

Although phosphorus and silicon alkalinity is included in the carbonate chemistry routines provided for OCMIP2 and OCMIP3 (Orr et al., 1999b; Aumont et al., 2004), those routines focused only on computing surface  $p\text{CO}_2$  and are now outdated. They have been replaced by *mocsy*, a Fortran 95

package for ocean modelers (Orr and Epitalon, 2015). Relative to the former OCMIP code, *mocsy* computes derived variables (e.g.,  $p\text{CO}_2$ , pH,  $\text{CO}_3^{2-}$ , and  $\text{CaCO}_3$  saturation states) throughout the water column, corrects for common errors in pressure corrections, and replaces the solver of the pH-alkalinity equation with the faster and safer SolveSaphe algorithm from Munhoven (2013). The latter converges under all conditions, even for very low salinity (low  $C_T$  and  $A_T$ ), unlike other approaches. Although by default *mocsy* uses older scales for temperature and salinity (ITS90 and PSS78, respectively) for input, it now includes a new option so that modelers can choose to use the TEOS-10 standards (Conservative Temperature and Absolute Salinity) instead. The *mocsy* routines may be downloaded from <https://github.com/jamesorr/mocsy.git>

### 3 Diagnostics

The second goal of OMIP-BGC is to provide a complete list of diagnostics requested for the ocean simulations of inert chemistry and biogeochemistry within the framework of OMIP and CMIP6. The limited diagnostics requested for the simulations of inert chemistry are provided in Table 4. The diagnostics requested for the biogeochemical simulations are more extensive. Hence they are given here as a series of tables separated by priority, type, and output frequency, i.e., as daily means (Table 5), annual means (Tables 6–9), and monthly means (Tables 10–17). The same list of requested variables is given in a different form and with



**Table 6.** Annual-mean biogeochemical output: priority 1.

Symbol	Variable name	Units	Shape	Priority	Long name
$C_T$	dissic	$\text{mol m}^{-3}$	XYZ	1	Dissolved inorganic carbon concentration
$C_T^{\text{nat}}$	dissicnat	$\text{mol m}^{-3}$	XYZ	1	Natural dissolved inorganic carbon concentration
$C_T^{\text{abio}}$	dissicabio	$\text{mol m}^{-3}$	XYZ	1	Abiotic dissolved inorganic carbon concentration
$^{14}C_T^{\text{abio}}$	dissi14cabio	$\text{mol m}^{-3}$	XYZ	1	Abiotic dissolved inorganic 14carbon concentration
$^{13}C_T$	dissi13c	$\text{mol m}^{-3}$	XYZ	1	Dissolved inorganic 13carbon concentration
$A_T$	talk	$\text{mol m}^{-3}$	XYZ	1	Total alkalinity
$A_T^{\text{nat}}$	talknat	$\text{mol m}^{-3}$	XYZ	1	Natural total alkalinity
pH	ph	1	XYZ	1	pH
$\text{pH}^{\text{nat}}$	phnat	1	XYZ	1	Natural pH
$\text{pH}^{\text{abio}}$	phabio	1	XYZ	1	Abiotic pH
$O_2$	o2	$\text{mol m}^{-3}$	XYZ	1	Dissolved oxygen concentration
$\text{NO}_3^-$	no3	$\text{mol m}^{-3}$	XYZ	1	Dissolved nitrate concentration
$P_T$	po4 <sup>a,b</sup>	$\text{mol m}^{-3}$	XYZ	1	Total dissolved inorganic phosphorus concentration
$Si_T$	si <sup>c</sup>	$\text{mol m}^{-3}$	XYZ	1	Total dissolved inorganic silicon concentration
Fe	dfe <sup>d</sup>	$\text{mol m}^{-3}$	XYZ	1	Mole concentration of dissolved iron in seawater
Chl	chl <sup>e</sup>	$\text{kg m}^{-3}$	XYZ	1	Mass concentration of total chlorophyll in seawater
$F_{\text{CO}_2^{\text{tot}}}$	fgco2	$\text{kg m}^{-2} \text{s}^{-1}$	XY	1	Surface downward flux of total $\text{CO}_2$
$F_{\text{CO}_2^{\text{nat}}}$	fgco2nat	$\text{kg m}^{-2} \text{s}^{-1}$	XY	1	Surface downward flux of natural $\text{CO}_2$
$F_{\text{CO}_2^{\text{abio}}}$	fgco2abio	$\text{kg m}^{-2} \text{s}^{-1}$	XY	1	Surface downward flux of abiotic $\text{CO}_2$
$F_{^{14}\text{CO}_2^{\text{abio}}}$	fg14co2abio	$\text{kg m}^{-2} \text{s}^{-1}$	XY	1	Surface downward flux of abiotic $^{14}\text{CO}_2$
$F_{^{13}\text{CO}_2}$	fg13co2	$\text{kg m}^{-2} \text{s}^{-1}$	XY	1	Surface downward flux of $^{13}\text{CO}_2$

<sup>a</sup> For models that do not carry  $P_T$  as a tracer, it should be computed from  $\text{NO}_3^-$  assuming N : P = 16 : 1; <sup>b</sup>  $P_T = \text{H}_3\text{PO}_4 + \text{H}_2\text{PO}_4^- + \text{HPO}_4^{2-} + \text{PO}_4^{3-}$ . In seawater most  $P_T$  is in the form of  $\text{HPO}_4^{2-}$ , while  $\text{PO}_4^{3-}$  makes up only  $\sim 10\%$  at pH 8. <sup>c</sup>  $Si_T = [\text{Si}(\text{OH})_4] + [\text{SiO}(\text{OH})_3^-]$ , dominated by the former (silicic acid). <sup>d</sup> Modeled dissolved iron includes all simulated dissolved species, both free and organically complexed. <sup>e</sup> Sum of chlorophyll from all phytoplankton group concentrations. In most models this is equal to chl<sub>diat</sub> + chl<sub>misc</sub>.

more detail in the OMIP-BGC MIP tables for CMIP6, which are available from <https://earthsystemcog.org/projects/wip/CMIP6DataRequest>.

Conceptually there is no difference in output requirements for the forced ocean simulations made for OMIP and the coupled simulations made with the ESMs that are participating in CMIP6 (e.g., DECK and historical). These simulations differ in forcing but not in the types of output requested.

To foster analysis of the model output generated by OMIP and CMIP6, OMIP-BGC plans to encourage contributions to a centralized list of analysis subprojects. The aim is to promote collaboration while avoiding excessive redundancy to allow the international community to advance more quickly and to exploit a greater diversity of output. Although much analysis will be led by OMIP members, others will also be encouraged to participate, e.g., scientists from other CMIP6 projects (e.g., C4MIP) or projects outside of CMIP (e.g., FishMIP or MAREMIP).

## 4 Conclusions

The required OMIP simulation (*omip1*) will be performed by many groups, each of which will couple their global-ocean, sea-ice model to a passive-tracer transport model for inert chemistry and ocean biogeochemistry, online. All groups, even those without biogeochemistry, will include at least one inert chemistry tracer (CFC-12) to assess subsurface model ventilation; two other tracers (CFC-11 and  $\text{SF}_6$ ) are also requested to better assess subsurface watermass ages relative to observations. Groups with ocean biogeochemical models should also include that component (OMIP-BGC). The physical component will be forced with the CORE II forcing (1948–2009) over five repeated cycles (310 years) as described in the companion OMIP paper (Griffies et al., 2016). The biogeochemical component will be connected for the full 310 years. Each model's atmospheric  $\text{CO}_2$  will be held to the CMIP6 preindustrial level (1 January 1850) during the first 150 years (1700–1849), while for the next 160 years (1850–2009) models will be forced to follow the historical obser-

**Table 7.** Annual-mean biogeochemical output: priority 2 (concentrations).

Symbol	Variable name	Units	Shape	Priority	Long name
DOC	dissoc	$\text{mol m}^{-3}$	XYZ	2	Dissolved organic carbon concentration
	phyc	$\text{mol m}^{-3}$	XYZ	2	Phytoplankton carbon concentration
	zooc	$\text{mol m}^{-3}$	XYZ	2	Zooplankton carbon concentration
	detoc	$\text{mol m}^{-3}$	XYZ	2	Detrital organic carbon concentration
$[\text{CaCO}_3]_{\text{calc}}$	calc	$\text{mol m}^{-3}$	XYZ	2	Calcite concentration
$[\text{CaCO}_3]_{\text{arag}}$	arag	$\text{mol m}^{-3}$	XYZ	2	Aragonite concentration
$[\text{O}_2]_{\text{sat}}$	o2sat	$\text{mol m}^{-3}$	XYZ	2	Dissolved oxygen concentration at saturation
$[\text{NH}_4^+]$	nh4	$\text{mol m}^{-3}$	XYZ	2	Dissolved ammonium concentration
	chldiat <sup>a</sup>	$\text{kg m}^{-3}$	XYZ	2	Mass concentration of diatoms expressed as chlorophyll in seawater
	chldiaz <sup>b</sup>	$\text{kg m}^{-3}$	XYZ	2	Mass concentration of diazotrophs expressed as chlorophyll in seawater
	chlcalc <sup>c</sup>	$\text{kg m}^{-3}$	XYZ	2	Mass concentration of calcareous phytoplankton expressed as chlorophyll in seawater
	chlpico <sup>d</sup>	$\text{kg m}^{-3}$	XYZ	2	Mass concentration of picophytoplankton expressed as chlorophyll in seawater
	chlmisc <sup>e</sup>	$\text{kg m}^{-3}$	XYZ	2	Mass concentration of other phytoplankton expressed as chlorophyll in seawater
	pon	$\text{mol m}^{-3}$	XYZ	2	Mole concentration of particulate organic matter expressed as nitrogen in seawater
	pop	$\text{mol m}^{-3}$	XYZ	2	Mole concentration of particulate organic matter expressed as phosphorus in seawater
	bfe <sup>f</sup>	$\text{mol m}^{-3}$	XYZ	2	Mole concentration of particulate organic matter expressed as iron in seawater
	bsi <sup>g</sup>	$\text{mol m}^{-3}$	XYZ	2	Mole concentration of particulate organic matter expressed as silicon in seawater
	phyn	$\text{mol m}^{-3}$	XYZ	2	Mole concentration of total phytoplankton expressed as nitrogen in seawater
	phyp	$\text{mol m}^{-3}$	XYZ	2	Mole concentration of total phytoplankton expressed as phosphorus in seawater
	phyfe	$\text{mol m}^{-3}$	XYZ	2	Mole concentration of total phytoplankton expressed as iron in seawater
	physi	$\text{mol m}^{-3}$	XYZ	2	Mole concentration of total phytoplankton expressed as silicon in seawater
DMS	dms	$\text{mol m}^{-3}$	XYZ	2	Mole concentration of dimethyl sulfide in seawater
$[\text{CO}_3^{2-}]$	co3	$\text{mol m}^{-3}$	XYZ	2	Carbonate ion concentration
$[\text{CO}_3^{2-}]^{\text{nat}}$	co3nat	$\text{mol m}^{-3}$	XYZ	2	Natural carbonate ion concentration
$[\text{CO}_3^{2-}]^{\text{abio}}$	co3abio	$\text{mol m}^{-3}$	XYZ	2	Abiotic carbonate ion concentration
$[\text{CO}_3^{2-}]_{\text{sat}}^{\text{calc}}$	co3satcalc	$\text{mol m}^{-3}$	XYZ	2	Carbonate ion concentration for seawater in equilibrium with pure calcite
$[\text{CO}_3^{2-}]_{\text{sat}}^{\text{arag}}$	co3satarag	$\text{mol m}^{-3}$	XYZ	2	Carbonate ion concentration for seawater in equilibrium with pure aragonite

<sup>a</sup> Chlorophyll from the diatom phytoplankton component concentration alone; <sup>b</sup> chlorophyll concentration from the diazotrophic phytoplankton component alone; <sup>c</sup> chlorophyll concentration from the calcite-producing phytoplankton component alone; <sup>d</sup> chlorophyll concentration from the picophytoplankton (< 2 µm) component alone; <sup>e</sup> chlorophyll from additional phytoplankton component concentrations alone; <sup>f</sup> sum of particulate organic iron component concentrations; <sup>g</sup> sum of particulate silica component concentrations.

**Table 8.** Annual-mean biogeochemical output: priority 2 (rates).

Variable name	Units	Shape	Priority	Long name
pp	$\text{mol m}^{-3} \text{s}^{-1}$	XYZ	2	Primary carbon production by total phytoplankton
pnitrate	$\text{mol m}^{-3} \text{s}^{-1}$	XYZ	2	Primary carbon production by phytoplankton due to nitrate uptake alone
pbfe	$\text{mol m}^{-3} \text{s}^{-1}$	XYZ	2	Biogenic iron production
pbsi	$\text{mol m}^{-3} \text{s}^{-1}$	XYZ	2	Biogenic silica production
pcalc	$\text{mol m}^{-3} \text{s}^{-1}$	XYZ	2	Calcite production
parag	$\text{mol m}^{-3} \text{s}^{-1}$	XYZ	2	Aragonite production
expc	$\text{mol m}^{-2} \text{s}^{-1}$	XYZ	2	Sinking particulate organic carbon flux
expn	$\text{mol m}^{-2} \text{s}^{-1}$	XYZ	2	Sinking particulate organic nitrogen flux
expp	$\text{mol m}^{-2} \text{s}^{-1}$	XYZ	2	Sinking particulate organic phosphorus flux
expfe	$\text{mol m}^{-2} \text{s}^{-1}$	XYZ	2	Sinking particulate iron flux
expsi	$\text{mol m}^{-2} \text{s}^{-1}$	XYZ	2	Sinking particulate silica flux
expcalc	$\text{mol m}^{-2} \text{s}^{-1}$	XYZ	2	Sinking calcite flux
exparag	$\text{mol m}^{-2} \text{s}^{-1}$	XYZ	2	Sinking aragonite flux
remoc	$\text{mol m}^{-3} \text{s}^{-1}$	XYZ	2	Remineralization of organic carbon
dcalc	$\text{mol m}^{-3} \text{s}^{-1}$	XYZ	2	Calcite dissolution
darag	$\text{mol m}^{-3} \text{s}^{-1}$	XYZ	2	Aragonite dissolution
ppdiat	$\text{mol m}^{-3} \text{s}^{-1}$	XYZ	2	Diatom primary carbon production

variations as defined for CMIP6. Physical analyses will focus on the fifth cycle, while those for the chemistry and biogeochemistry will also study transient changes over the industrial era. All OMIP-BGC simulations should include either the *natural* carbon tracer  $C_T^{\text{nat}}$ , or a parallel separate simulation that accounts only for natural carbon, in order to assess and remove effects of model drift.

An optional simulation (*omip1-spunup*) is requested from all groups having biogeochemistry and able to afford a long spin-up, made beforehand. Rather than using observed climatologies to initialize the biogeochemistry as in *omip1*, this simulation will be initialized with model tracer fields that have been spun up preferably for 2000 years or more. In addition, the *omip1-spunup* simulation (and its spin-up) will include two simplified tracers, abiotic carbon and radiocarbon, to evaluate deep-ocean circulation and deconvolve physical vs. biological contributions to the carbon cycle. Finally, groups already having  $^{13}\text{C}$  as a biogeochemical tracer are encouraged to include that in the *omip1-spunup* simulation (and its spin-up), using common OMIP formulations for gas exchange and fractionation, to evaluate the simulated Suess effect and to compare cycling of  $^{13}\text{C}$  in the marine ecosystem. Besides the initial fields and the three new tracers, the *omip1* and *omip1-spunup* simulation protocols are identical.

**Code and data availability.** To facilitate comparison, an OMIP-BGC web page (<http://omip-bgc.lscce.ipsl.fr>) provides links to these protocols as well as links for OMIP-BGC's common atmospheric gas histories, data fields for initialization, and code to compute all facets of gas exchange and carbonate chemistry. Eventually, all input data files will be available directly from input4mips (<https://esgf-node.llnl.gov/search/input4mips>). The code mentioned here is available in the *mocsy* package, which can be obtained as detailed in Sect. 2.6. That package contains the carbonate chemistry routines as well as routines in its *gasx* module to compute Schmidt numbers, solubilities, and air–sea exchange for the gases to be modeled during OMIP ( $\text{CO}_2$ ,  $\text{O}_2$ , CFC-11, CFC-12, and  $\text{SF}_6$ ).

**Table 9.** Annual-mean biogeochemical output: priority 3.

Variable name	Units	Shape	Priority	Long name
bacc	$\text{mol m}^{-3}$	XYZ	3	Bacterial carbon concentration
phydiat	$\text{mol m}^{-3}$	XYZ	3	Mole concentration of diatoms expressed as carbon in seawater
phydiaz	$\text{mol m}^{-3}$	XYZ	3	Mole conc. of diazotrophs expressed as carbon in seawater
phycalc	$\text{mol m}^{-3}$	XYZ	3	Mole conc. of calcareous phytoplankton expressed as carbon in seawater
phypico <sup>a</sup>	$\text{mol m}^{-3}$	XYZ	3	Mole conc. of picophytoplankton expressed as carbon in seawater
phymisc <sup>b</sup>	$\text{mol m}^{-3}$	XYZ	3	Mole conc. of miscellaneous phytoplankton expressed as carbon in seawater
zmicro <sup>c</sup>	$\text{mol m}^{-3}$	XYZ	3	Mole conc. of microzooplankton expressed as carbon in seawater
zmeso <sup>d</sup>	$\text{mol m}^{-3}$	XYZ	3	Mole conc. of mesozooplankton expressed as carbon in seawater
zmisc <sup>e</sup>	$\text{mol m}^{-3}$	XYZ	3	Mole conc. of other zooplankton expressed as carbon in seawater
dpocdtdiaz	$\text{mol m}^{-3} \text{ s}^{-1}$	XYZ	3	Tendency of mole conc. of organic carbon in seawater due to NPP by diazotrophs
dpocdtcalc	$\text{mol m}^{-3} \text{ s}^{-1}$	XYZ	3	Tendency of mole conc. of organic carbon in seawater due to NPP by calcareous phytoplankton
dpocdtpico	$\text{mol m}^{-3} \text{ s}^{-1}$	XYZ	3	Tendency of mole conc. of organic carbon in seawater due to NPP by picophytoplankton
ppdiat	$\text{mol m}^{-3} \text{ s}^{-1}$	XYZ	3	Net primary organic carbon production by diatoms
ppdiaz	$\text{mol m}^{-3} \text{ s}^{-1}$	XYZ	3	Net primary mole productivity of carbon by diazotrophs
ppcalc	$\text{mol m}^{-3} \text{ s}^{-1}$	XYZ	3	Net primary mole productivity of carbon by calcareous phytoplankton
pppico	$\text{mol m}^{-3} \text{ s}^{-1}$	XYZ	3	Net primary mole productivity of carbon by picophytoplankton
ppmisc	$\text{mol m}^{-3} \text{ s}^{-1}$	XYZ	3	Net primary organic carbon production by other phytoplankton
bddtdic	$\text{mol m}^{-3} \text{ s}^{-1}$	XYZ	3	Rate of change in dissolved inorganic carbon due to biological activity
bddtdin	$\text{mol m}^{-3} \text{ s}^{-1}$	XYZ	3	Rate of change in nitrogen nutrients due to biological activity
bddtdip	$\text{mol m}^{-3} \text{ s}^{-1}$	XYZ	3	Rate of change in dissolved phosphorus due to biological activity
bddtdife	$\text{mol m}^{-3} \text{ s}^{-1}$	XYZ	3	Rate of change in dissolved inorganic iron due to biological activity
bddtdisi	$\text{mol m}^{-3} \text{ s}^{-1}$	XYZ	3	Rate of change in total dissolved inorganic silicon due to biological activity
bddtalk	$\text{mol m}^{-3} \text{ s}^{-1}$	XYZ	3	Rate of change in alkalinity due to biological activity
fescav	$\text{mol m}^{-3} \text{ s}^{-1}$	XYZ	3	Nonbiogenic iron scavenging
fediss	$\text{mol m}^{-3} \text{ s}^{-1}$	XYZ	3	Particle source of dissolved iron
graz	$\text{mol m}^{-3} \text{ s}^{-1}$	XYZ	3	Total grazing of phytoplankton by zooplankton

<sup>a</sup> Carbon concentration from the picophytoplankton ( $< 2 \mu\text{m}$ ) component alone; <sup>b</sup> carbon concentration from the additional phytoplankton component alone; <sup>c</sup> carbon concentration from the microzooplankton ( $< 20 \mu\text{m}$ ) component alone; <sup>d</sup> carbon concentration from the mesozooplankton ( $20\text{--}200 \mu\text{m}$ ) component alone; <sup>e</sup> carbon from additional zooplankton component concentrations alone (e.g., micro, meso). Provides check for model intercomparison since some phytoplankton groups are supersets.

**Table 10.** Monthly mean biogeochemical output: priority 1.

Symbol	Variable name	Units	Shape	Priority	Long name
	dissicos	$\text{mol m}^{-3}$	XY	1	Surface dissolved inorganic carbon concentration
	dissicnatos	$\text{mol m}^{-3}$	XY	1	Surface natural dissolved inorganic carbon concentration
	dissicabioos	$\text{mol m}^{-3}$	XY	1	Surface abiotic dissolved inorganic carbon concentration
	dissi14cabioos	$\text{mol m}^{-3}$	XY	1	Surface abiotic dissolved inorganic $^{14}\text{C}$ carbon concentration
	dissi13cos	$\text{mol m}^{-3}$	XY	1	Surface dissolved inorganic $^{13}\text{C}$ carbon concentration
	talkos	$\text{mol m}^{-3}$	XY	1	Surface total alkalinity
	talknatos	$\text{mol m}^{-3}$	XY	1	Surface natural total alkalinity
	phos	1	XY	1	Surface pH on total scale
	sios	$\text{mol m}^{-3}$	XY	1	Surface total dissolved inorganic silicon concentration
	o2os	$\text{mol m}^{-3}$	XY	1	Surface dissolved oxygen concentration
	o2satos	$\text{mol m}^{-3}$	XY	1	Surface dissolved oxygen concentration at saturation
	po4os	$\text{mol m}^{-3}$	XY	1	Surface total dissolved inorganic phosphorus concentration
	chlos	$\text{kg m}^{-3}$	XY	1	Surface mass conc. of total phytoplankton expressed as chlorophyll in seawater
$C_T$	dissic	$\text{mol m}^{-3}$	XYZ	1	Dissolved inorganic carbon concentration
$A_T$	talk	$\text{mol m}^{-3}$	XYZ	1	Total alkalinity
pH	ph	1	XYZ	1	pH on total scale
$P_T$	po4 <sup>a</sup>	$\text{mol m}^{-3}$	XYZ	1	Total dissolved inorganic phosphorus concentration
	intpp <sup>b</sup>	$\text{mol m}^{-2} \text{s}^{-1}$	XY	1	Primary organic carbon production by all types of phytoplankton
	expc100 <sup>c</sup>	$\text{mol m}^{-2} \text{s}^{-1}$	XY	1	Downward flux of particle organic carbon
	expcalc100 <sup>b</sup>	$\text{mol m}^{-2} \text{s}^{-1}$	XY	1	Downward flux of calcite
	exparag100 <sup>b</sup>	$\text{mol m}^{-2} \text{s}^{-1}$	XY	1	Downward flux of aragonite
$p\text{CO}_2$	spco2	Pa	XY	1	Surface aqueous partial pressure of $\text{CO}_2$
$p\text{CO}_2^{\text{nat}}$	spco2nat	Pa	XY	1	Natural surface aqueous partial pressure of $\text{CO}_2$
$p\text{CO}_2^{\text{abio}}$	spco2abio	Pa	XY	1	Abiotic surface aqueous partial pressure of $\text{CO}_2$
$F_{\text{CO}_2^{\text{tot}}}$	fgco2	$\text{kg m}^{-2} \text{s}^{-1}$	XY	1	Surface downward flux of total $\text{CO}_2$
$F_{\text{CO}_2^{\text{nat}}}$	fgco2nat	$\text{kg m}^{-2} \text{s}^{-1}$	XY	1	Surface downward flux of natural $\text{CO}_2$
$F_{\text{CO}_2^{\text{abio}}}$	fgco2abio	$\text{kg m}^{-2} \text{s}^{-1}$	XY	1	Surface downward flux of abiotic $\text{CO}_2$
$F_{^{14}\text{CO}_2^{\text{abio}}}$	fg14co2abio	$\text{kg m}^{-2} \text{s}^{-1}$	XY	1	Surface downward flux of abiotic $^{14}\text{CO}_2$
$F_{^{13}\text{CO}_2}$	fg13co2	$\text{kg m}^{-2} \text{s}^{-1}$	XY	1	Surface downward flux of $^{13}\text{CO}_2$
$F_{\text{O}_2}$	fgo2	$\text{mol m}^{-2} \text{s}^{-1}$	XY	1	Surface downward flux of $\text{O}_2$

<sup>a</sup> For models that do not carry  $P_T$  as a tracer, compute it from  $\text{NO}_3^-$  assuming N:P = 16:1. <sup>b</sup> Vertically integrated total primary (organic carbon) production by phytoplankton. This should equal the sum of  $\text{intpdia} + \text{intpphymisc}$ , but those individual components may be unavailable in some models. <sup>c</sup> At 100 m depth.

**Table 11.** Monthly mean biogeochemical output: priority 2 (2-D fields).

Symbol	Variable name	Units	Shape	Priority	Long name
	dissocos	$\text{mol m}^{-3}$	XY	2	Surface dissolved organic carbon concentration
	phycos	$\text{mol m}^{-3}$	XY	2	Surface phytoplankton carbon concentration
	zoocos	$\text{mol m}^{-3}$	XY	2	Surface zooplankton carbon concentration
	detocos	$\text{mol m}^{-3}$	XY	2	Surface detrital organic carbon concentration
	calcos	$\text{mol m}^{-3}$	XY	2	Surface calcite concentration
	aragos	$\text{mol m}^{-3}$	XY	2	Surface aragonite concentration
	phnatos	1	XY	2	Surface natural pH on total scale
	phabioos	1	XY	2	Surface abiotic pH on total scale
	no3os	$\text{mol m}^{-3}$	XY	2	Surface dissolved nitrate concentration
	nh4os	$\text{mol m}^{-3}$	XY	2	Surface dissolved ammonium concentration
	dfeos	$\text{mol m}^{-3}$	XY	2	Surface dissolved iron concentration
	co3os	$\text{mol m}^{-3}$	XY	2	Surface carbonate ion concentration
	co3natos	$\text{mol m}^{-3}$	XY	2	Surface natural carbonate ion concentration
	co3abioos	$\text{mol m}^{-3}$	XY	2	Surface abiotic carbonate ion concentration
	co3satcalcos	$\text{mol m}^{-3}$	XY	2	Surface carbonate ion conc. for seawater in equilibrium with pure calcite
	co3sataragos	$\text{mol m}^{-3}$	XY	2	Surface carbonate ion conc. for seawater in equilibrium with pure aragonite
	limndiat <sup>f</sup>	1	XY	2	Nitrogen limitation of diatoms
	limirrdiat <sup>f</sup>	1	XY	2	Irradiance limitation of diatoms
	limfediat <sup>f</sup>	1	XY	2	Iron limitation of diatoms
	intppntrate <sup>a</sup>	$\text{mol m}^{-2} \text{s}^{-1}$	XY	2	Primary organic carbon production by phytoplankton based on nitrate uptake alone
	intppdiat <sup>b</sup>	$\text{mol m}^{-2} \text{s}^{-1}$	XY	2	Primary organic carbon production by diatoms
$\int C_T dz$	intdic <sup>c</sup>	$\text{kg m}^{-2}$	XY	2	Dissolved inorganic carbon content
$\int \text{DOC} dz$	intdoc <sup>d</sup>	$\text{kg m}^{-2}$	XY	2	Dissolved organic carbon content
$\int \text{OC} dz$	intpoc <sup>e</sup>	$\text{kg m}^{-2}$	XY	2	Particulate organic carbon content

<sup>a</sup> Vertically integrated primary (organic carbon) production by phytoplankton based on nitrate uptake alone;

<sup>b</sup> vertically integrated primary (organic carbon) production by the diatom phytoplankton component alone;

<sup>c</sup> vertically integrated  $C_T$ ;

<sup>d</sup> vertically integrated DOC (explicit pools only);

<sup>e</sup> vertically integrated POC;

<sup>f</sup> these 2-D limitation terms should be calculated as the carbon biomass weighted average for the upper 100 m.

**Table 12.** Monthly mean biogeochemical output: priority 2 (3-D fields).

Symbol	Variable name	Units	Shape	Priority	Long name
$C_T^{\text{nat}}$	dissicnat	$\text{mol m}^{-3}$	XYZ	2	Natural dissolved inorganic carbon concentration
$C_T^{\text{abio}}$	dissicabio	$\text{mol m}^{-3}$	XYZ	2	Abiotic dissolved inorganic carbon concentration
$^{14}C_T^{\text{abio}}$	dissi14cabio	$\text{mol m}^{-3}$	XYZ	2	Abiotic dissolved inorganic $^{14}\text{C}$ concentration
$^{13}C_T$	dissi13c	$\text{mol m}^{-3}$	XYZ	2	Dissolved inorganic $^{13}\text{C}$ concentration
$A_T^{\text{nat}}$	talknat	$\text{mol m}^{-3}$	XYZ	2	Natural total alkalinity
$\text{pH}^{\text{nat}}$	phnat	1	XYZ	2	Natural pH
$\text{pH}^{\text{abio}}$	phabio	1	XYZ	2	Abiotic pH
[O <sub>2</sub> ]	o2	$\text{mol m}^{-3}$	XYZ	2	Dissolved oxygen concentration
	o2sat	$\text{mol m}^{-3}$	XYZ	2	Dissolved oxygen concentration at saturation
[NO <sub>3</sub> <sup>-</sup> ]	no3	$\text{mol m}^{-3}$	XYZ	2	Dissolved nitrate concentration
[NH <sub>4</sub> <sup>+</sup> ]	nh4	$\text{mol m}^{-3}$	XYZ	2	Dissolved ammonium concentration
Fe <sup>c</sup>	dfe	$\text{mol m}^{-3}$	XYZ	2	Dissolved iron concentration
$Si_T$	si	$\text{mol m}^{-3}$	XYZ	2	Total dissolved inorganic silicon concentration
Chl	chl	$\text{kg m}^{-3}$	XYZ	2	Mass concentration of total phytoplankton expressed as chlorophyll in seawater
	DOC	$\text{mol m}^{-3}$	XYZ	2	Dissolved organic carbon concentration
	phyc	$\text{mol m}^{-3}$	XYZ	2	Phytoplankton carbon concentration
	zooc	$\text{mol m}^{-3}$	XYZ	2	Zooplankton carbon concentration
	detoc	$\text{mol m}^{-3}$	XYZ	2	Detrital organic carbon concentration
[CaCO <sub>3</sub> ] <sub>calc</sub>	calc	$\text{mol m}^{-3}$	XYZ	2	Calcite concentration
[CaCO <sub>3</sub> ] <sub>arag</sub>	arag	$\text{mol m}^{-3}$	XYZ	2	Aragonite concentration
[CO <sub>3</sub> <sup>2-</sup> ]	co3	$\text{mol m}^{-3}$	XYZ	2	Carbonate ion concentration
[CO <sub>3</sub> <sup>2-</sup> ] <sup>nat</sup>	co3nat	$\text{mol m}^{-3}$	XYZ	2	Natural carbonate ion concentration
[CO <sub>3</sub> <sup>2-</sup> ] <sup>abio</sup>	co3abio	$\text{mol m}^{-3}$	XYZ	2	Abiotic carbonate ion concentration
[CO <sub>3</sub> <sup>2-</sup> ] <sub>sat</sub> <sup>calc</sup>	co3satcalc	$\text{mol m}^{-3}$	XYZ	2	Carbonate ion concentration for seawater in equilibrium with pure calcite
[CO <sub>3</sub> <sup>2-</sup> ] <sub>sat</sub> <sup>arag</sup>	co3satarag	$\text{mol m}^{-3}$	XYZ	2	Carbonate ion concentration for seawater in equilibrium with pure aragonite



**Table 13.** Monthly mean biogeochemical output: priority 3 (concentrations of surface fields).

Variable name	Units	Shape	Priority	Long name
baccos	$\text{mol m}^{-3}$	XY	3	Surface bacterial carbon concentration
phydiatos	$\text{mol m}^{-3}$	XY	3	Surface mole concentration of diatoms expressed as carbon in seawater
phydiazos	$\text{mol m}^{-3}$	XY	3	Surface mole concentration of diazotrophs expressed as carbon in seawater
phycalcos	$\text{mol m}^{-3}$	XY	3	Surface mole concentration of calcareous phytoplankton expressed as carbon in seawater
phypicoos	$\text{mol m}^{-3}$	XY	3	Surface mole concentration of picophytoplankton expressed as carbon in seawater
phymiscos	$\text{mol m}^{-3}$	XY	3	Surface mole concentration of miscellaneous phytoplankton expressed as carbon in seawater
zmicroos	$\text{mol m}^{-3}$	XY	3	Surface mole concentration of microzooplankton expressed as carbon in seawater
zmesoos	$\text{mol m}^{-3}$	XY	3	Surface mole concentration of mesozooplankton expressed as carbon in seawater
zmiscos	$\text{mol m}^{-3}$	XY	3	Surface mole concentration of other zooplankton expressed as carbon in seawater
chldiats	$\text{kg m}^{-3}$	XY	3	Surface mass concentration of diatoms expressed as chlorophyll in seawater
chldiazos	$\text{kg m}^{-3}$	XY	3	Surface mass concentration of diazotrophs expressed as chlorophyll in seawater
chlcalcos	$\text{kg m}^{-3}$	XY	3	Surface mass concentration of calcareous phytoplankton expressed as chlorophyll in seawater
chlpicoos	$\text{kg m}^{-3}$	XY	3	Surface mass concentration of picophytoplankton expressed as chlorophyll in seawater
chlmiscos	$\text{kg m}^{-3}$	XY	3	Surface mass concentration of other phytoplankton expressed as chlorophyll in seawater
ponos	$\text{mol m}^{-3}$	XY	3	Surface mole concentration of particulate organic matter expressed as nitrogen in seawater
popos	$\text{mol m}^{-3}$	XY	3	Surface mole concentration of particulate organic matter expressed as phosphorus in seawater
bfeos	$\text{mol m}^{-3}$	XY	3	Surface mole concentration of particulate organic matter expressed as iron in seawater
bsios	$\text{mol m}^{-3}$	XY	3	Surface mole concentration of particulate organic matter expressed as silicon in seawater
phynos	$\text{mol m}^{-3}$	XY	3	Surface mole concentration of phytoplankton nitrogen in seawater
phypos	$\text{mol m}^{-3}$	XY	3	Surface mole concentration of total phytoplankton expressed as phosphorus in seawater
phyfeos	$\text{mol m}^{-3}$	XY	3	Surface mass concentration of diazotrophs expressed as chlorophyll in seawater
physios	$\text{mol m}^{-3}$	XY	3	Surface mole concentration of total phytoplankton expressed as silicon in seawater
dmsos	$\text{mol m}^{-3}$	XY	3	Surface mole concentration of dimethyl sulfide in seawater

**Table 14.** Monthly mean biogeochemical output: priority 3 (concentrations of 3-D fields).

Variable name	Units	Shape	Priority	Long name
bacc	$\text{mol m}^{-3}$	XYZ	3	Bacterial carbon concentration
phydiat	$\text{mol m}^{-3}$	XYZ	3	Mole concentration of diatoms expressed as carbon in seawater
phydiaz	$\text{mol m}^{-3}$	XYZ	3	Mole concentration of diazotrophs expressed as carbon in seawater
phycalc	$\text{mol m}^{-3}$	XYZ	3	Mole concentration of calcareous phytoplankton expressed as carbon in seawater
phypico	$\text{mol m}^{-3}$	XYZ	3	Mole concentration of picophytoplankton expressed as carbon in seawater
phymisc	$\text{mol m}^{-3}$	XYZ	3	Mole concentration of miscellaneous phytoplankton expressed as carbon in seawater
zmicro	$\text{mol m}^{-3}$	XYZ	3	Mole concentration of microzooplankton expressed as carbon in seawater
zmeso	$\text{mol m}^{-3}$	XYZ	3	Mole concentration of mesozooplankton expressed as carbon in seawater
zmisc	$\text{mol m}^{-3}$	XYZ	3	Mole concentration of other zooplankton expressed as carbon in seawater
chldiat	$\text{kg m}^{-3}$	XYZ	3	Mass concentration of diatoms expressed as chlorophyll in seawater
chldiaz	$\text{kg m}^{-3}$	XYZ	3	Mass concentration of diazotrophs expressed as chlorophyll in seawater
chlcalc	$\text{kg m}^{-3}$	XYZ	3	Mass concentration of calcareous phytoplankton expressed as chlorophyll in seawater
chlpico	$\text{kg m}^{-3}$	XYZ	3	Mass concentration of picophytoplankton expressed as chlorophyll in seawater
chlmisc	$\text{kg m}^{-3}$	XYZ	3	Mass concentration of other phytoplankton expressed as chlorophyll in seawater
pon	$\text{mol m}^{-3}$	XYZ	3	Mole concentration of particulate organic matter expressed as nitrogen in seawater
pop	$\text{mol m}^{-3}$	XYZ	3	Mole concentration of particulate organic matter expressed as phosphorus in seawater
bfe	$\text{mol m}^{-3}$	XYZ	3	Mole concentration of particulate organic matter expressed as iron in seawater
bsi	$\text{mol m}^{-3}$	XYZ	3	Mole concentration of particulate organic matter expressed as silicon in seawater
phyn	$\text{mol m}^{-3}$	XYZ	3	Mole concentration of phytoplankton nitrogen in seawater
phyp	$\text{mol m}^{-3}$	XYZ	3	Mole concentration of total phytoplankton expressed as phosphorus in seawater
phyfe	$\text{mol m}^{-3}$	XYZ	3	Mass concentration of diazotrophs expressed as chlorophyll in seawater
physi	$\text{mol m}^{-3}$	XYZ	3	Mole concentration of total phytoplankton expressed as silicon in seawater
dms	$\text{mol m}^{-3}$	XYZ	3	Mole concentration of dimethyl sulfide in seawater

**Table 15.** Monthly mean biogeochemical output: priority 3 (gas exchange, river, burial,  $\text{N}_2$  fixation, thresholds).

Symbol	Variable name	Units	Shape	Priority	Long name
$\Delta p\text{CO}_2$	dpco2 <sup>a</sup>	Pa	XY	3	Delta pCO <sub>2</sub>
$\Delta p\text{CO}_2^{\text{nat}}$	dpco2nat <sup>a</sup>	Pa	XY	3	Natural delta pCO <sub>2</sub>
$\Delta p\text{CO}_2^{\text{abio}}$	dpco2abio <sup>a</sup>	Pa	XY	3	Abiotic delta pCO <sub>2</sub>
$\Delta p\text{O}_2$	dpo2 <sup>b</sup>	Pa	XY	3	Delta pO <sub>2</sub>
$F_{\text{DMS}}$	fgdms	$\text{mol m}^{-2} \text{ s}^{-1}$	XY	3	Surface upward flux of DMS
	icfriver	$\text{mol m}^{-2} \text{ s}^{-1}$	XY	3	Flux of inorganic carbon into ocean surface by runoff
	fric	$\text{mol m}^{-2} \text{ s}^{-1}$	XY	3	Downward inorganic carbon flux at ocean bottom
	ocfriver	$\text{mol m}^{-2} \text{ s}^{-1}$	XY	3	Flux of organic carbon into ocean surface by runoff
	froc	$\text{mol m}^{-2} \text{ s}^{-1}$	XY	3	Downward organic carbon flux at ocean bottom
	intpn2	$\text{mol m}^{-2} \text{ s}^{-1}$	XY	3	Nitrogen fixation rate in ocean
	fsn	$\text{mol m}^{-2} \text{ s}^{-1}$	XY	3	Surface downward net flux of nitrogen
	frn	$\text{mol m}^{-2} \text{ s}^{-1}$	XY	3	Nitrogen loss to sediments and through denitrification
	fsfe	$\text{mol m}^{-2} \text{ s}^{-1}$	XY	3	Surface downward net flux of iron
	frfe	$\text{mol m}^{-2} \text{ s}^{-1}$	XY	3	Iron loss to sediments
CSH	o2min	$\text{mol m}^{-3}$	XY	3	Oxygen minimum concentration
	zo2min	m	XY	3	Depth of oxygen minimum concentration
ASH	zsatcalc <sup>c</sup>	m	XY	3	Calcite saturation depth
	zsatarag <sup>d</sup>	m	XY	3	Aragonite saturation depth

<sup>a</sup> Difference between atmospheric and oceanic partial pressure of  $\text{CO}_2$  (positive meaning ocean > atmosphere); <sup>b</sup> difference between atmospheric and oceanic partial pressure of  $\text{O}_2$  (positive meaning ocean > atmosphere); <sup>c</sup> depth of calcite saturation horizon (0 if < surface, “missing” if > bottom; if 2, then the shallower); <sup>d</sup> depth of the aragonite saturation horizon (0 if < surface, “missing” if > bottom; if 2, then the shallower).

**Table 16.** Monthly mean biogeochemical output: priority 3 (production and rates of change).

Variable name	Units	Shape	Priority	Long name
expn100 <sup>a</sup>	$\text{mol m}^{-2} \text{s}^{-1}$	XY	3	Downward flux of particulate nitrogen
expp100 <sup>a</sup>	$\text{mol m}^{-2} \text{s}^{-1}$	XY	3	Downward flux of particulate phosphorus
expfe100 <sup>a</sup>	$\text{mol m}^{-2} \text{s}^{-1}$	XY	3	Downward flux of particulate iron
expsi100 <sup>a</sup>	$\text{mol m}^{-2} \text{s}^{-1}$	XY	3	Downward flux of particulate silica
fddtdic <sup>b</sup>	$\text{mol m}^{-2} \text{s}^{-1}$	XY	3	Rate of change in net dissolved inorganic carbon
fddtdin <sup>b,c</sup>	$\text{mol m}^{-2} \text{s}^{-1}$	XY	3	Rate of change in net dissolved inorganic nitrogen
fddtdip <sup>b</sup>	$\text{mol m}^{-2} \text{s}^{-1}$	XY	3	Rate of change in net dissolved inorganic phosphorus
fddtdife <sup>b</sup>	$\text{mol m}^{-2} \text{s}^{-1}$	XY	3	Rate of change in net dissolved inorganic iron
fddtdisi <sup>b</sup>	$\text{mol m}^{-2} \text{s}^{-1}$	XY	3	Rate of change in net dissolved inorganic silicon
fddtalk <sup>b</sup>	$\text{mol m}^{-2} \text{s}^{-1}$	XY	3	Rate of change in total alkalinity
fbddtdic <sup>b</sup>	$\text{mol m}^{-2} \text{s}^{-1}$	XY	3	Rate of change in dissolved inorganic carbon due to biological activity
fbddtdin <sup>b,d</sup>	$\text{mol m}^{-2} \text{s}^{-1}$	XY	3	Rate of change in dissolved inorganic nitrogen due to biological activity
fbddtdip <sup>b</sup>	$\text{mol m}^{-2} \text{s}^{-1}$	XY	3	Rate of change in total dissolved inorganic phosphorus due to biological activity
fbddtdife <sup>b</sup>	$\text{mol m}^{-2} \text{s}^{-1}$	XY	3	Rate of change in dissolved inorganic iron due to biological activity
fbddtdisi <sup>b</sup>	$\text{mol m}^{-2} \text{s}^{-1}$	XY	3	Rate of change in total dissolved inorganic silicon due to biological activity

<sup>a</sup> At 100 m depth; <sup>b</sup> integral over upper 100 m only; <sup>c</sup> net time rate of change in nitrogen nutrients (e.g.,  $\text{NO}_3^- + \text{NH}_4^+$ ); <sup>d</sup> vertical integral of net biological terms in time rate of change in nitrogen nutrients (e.g.,  $\text{NO}_3^- + \text{NH}_4^+$ ).

**Table 17.** Monthly mean biogeochemical output: priority 3 (production, grazing, sinking, limitation).

Variable name	Units	Shape	Priority	Long name
pp	$\text{mol m}^{-3} \text{s}^{-1}$	XYZ	3	Primary carbon production by phytoplankton
graz	$\text{mol m}^{-3} \text{s}^{-1}$	XYZ	3	Total grazing of phytoplankton by zooplankton
expc	$\text{mol m}^{-2} \text{s}^{-1}$	XY	3	Sinking particulate organic carbon flux
limndiaz	1	XY	3	Nitrogen limitation of diazotrophs
limncalc	1	XY	3	Nitrogen limitation of calcareous phytoplankton
limnpico	1	XY	3	Nitrogen limitation of picophytoplankton
limnmisc	1	XY	3	Nitrogen limitation of other phytoplankton
limirrdiaz	1	XY	3	Irradiance limitation of diazotrophs
limirrcalc	1	XY	3	Irradiance limitation of calcareous phytoplankton
limirrpico	1	XY	3	Irradiance limitation of picophytoplankton
limirmisc	1	XY	3	Irradiance limitation of other phytoplankton
limfediaz	1	XY	3	Iron limitation of diazotrophs
limfecalc	1	XY	3	Iron limitation of calcareous phytoplankton
limfepico	1	XY	3	Iron limitation of picophytoplankton
limfemisc	1	XY	3	Iron limitation of other phytoplankton
intppdiaz	$\text{mol m}^{-2} \text{s}^{-1}$	XY	3	Net primary mole productivity of carbon by diazotrophs
intppcalc	$\text{mol m}^{-2} \text{s}^{-1}$	XY	3	Net primary mole productivity of carbon by calcareous phytoplankton
intpppico	$\text{mol m}^{-2} \text{s}^{-1}$	XY	3	Net primary mole productivity of carbon by picophytoplankton
intppmisc	$\text{mol m}^{-2} \text{s}^{-1}$	XY	3	Net primary organic carbon production by other phytoplankton
intpbn	$\text{mol m}^{-2} \text{s}^{-1}$	XY	3	Nitrogen production
intpbp	$\text{mol m}^{-2} \text{s}^{-1}$	XY	3	Phosphorus production
intpbfe	$\text{mol m}^{-2} \text{s}^{-1}$	XY	3	Iron production
intpbsi	$\text{mol m}^{-2} \text{s}^{-1}$	XY	3	Silica production
intpcalcite	$\text{mol m}^{-2} \text{s}^{-1}$	XY	3	Calcite production
intparag	$\text{mol m}^{-2} \text{s}^{-1}$	XY	3	Aragonite production

## Appendix A: Converting modeled $^{14}\text{C}$ fluxes to conventional units

The  $^{14}\text{C}$  tracer that is adopted for OMIP from OCMIP is fractionation corrected to avoid the need to explicitly compute  $^{13}\text{C}$  fluxes between modeled carbon reservoirs. It is also normalized. Both of these manipulations affect the units of modeled  $^{14}\text{C}$  concentrations and fluxes. These normalized, fractionation-corrected units must be used when OMIP model groups save their  $^{14}\text{C}$  output. The saved OMIP model output is used directly to calculate simulated  $\Delta^{14}\text{C}_{\text{ocn}}$  with Eqs. (29) and (30) for comparison to observations, but for budget calculations it must be converted to atoms or moles of  $^{14}\text{C}$  (Naegler, 2009). Here we detail that conversion.

As mentioned in Sect. 2.5.3 and 2.5.4, modeled  $^{14}\text{C}$  ratios in OMIP are expressed relative to total carbon, i.e., the *fractional isotopic abundance*  $^{14}r_{\text{model}} = ^{14}\text{C}/\text{C}$ ; conversely, for  $^{13}\text{C}$ , its ratio is typically shown relative to  $^{12}\text{C}$  (Mook, 1986), i.e., with the *isotopic ratio*  $^{13}R = ^{13}\text{C}/^{12}\text{C}$ . The *fractional abundance* approach is convenient for ocean carbon-cycle models, which already transport total carbon, e.g., to assess uptake of fossil  $\text{CO}_2$ , which includes both  $^{12}\text{C}$  and  $^{13}\text{C}$ . But whether  $^{12}\text{C}$  or  $\text{C}$  is the reference, there is only a small effect on simulated results. That is,  $^{13}\text{C}$  amounts to only about 1 % of the total carbon ( $^{13}R_{\text{std}} = 0.0112372$ , Craig, 1957) and  $^{14}\text{C}$  is proportionally much less still. For  $^{14}\text{C}$ , we adopt as a reference the standard isotopic fractional abundance  $^{14}r_{\text{std}}$  ( $^{14}\text{C}/\text{C}$ ) of  $1.170 \times 10^{-12}$ , which follows from the absolute international standard activity for  $^{14}r_{\text{std}}$  of  $13.56 \pm 0.07$  disintegrations per minute (dpm) per g C (Karlen et al., 1965) and a radiocarbon half-life of  $5700 \pm 30$  years (Audi et al., 2003; Bé et al., 2013). For comparison, Karlen et al. (1965) used the now outdated value for the half-life ( $5730 \pm 40$  years, Godwin, 1962) to infer that  $^{14}r_{\text{std}} = 1.176 \times 10^{-12}$ ; both of those values should now be revised downward to the values provided in the previous sentence.

The purpose of  $\Delta^{14}\text{C}$  and the fractionation-normalized ratio  $^{14}r_N$  is to remove the impact of isotopic fractionation to isolate the effect of “aging” by radioactive decay. Such fractionation occurs during photosynthesis and air–sea  $\text{CO}_2$  exchange, leading to differences in the  $^{13}\text{C}/^{12}\text{C}$  signature in different reservoirs; without fractionation, that ratio would not differ between carbon reservoirs. Fractionation of  $^{14}\text{C}$  is about twice that of  $^{13}\text{C}$  in permil units, based on the atomic mass difference relative to  $^{12}\text{C}$ . One can approximately remove the influence of fractionation on  $^{14}\text{C}$  by relying on measured  $\delta^{13}\text{C}$  referenced to a common isotopic  $\delta^{13}\text{C}$  signature, taken as  $-25\text{‰}$  (Broecker and Olson, 1961). Thus for a particular reservoir  $i$  where  $^{14}r_i = ^{14}\text{C}/\text{C}$ ,

$$^{14}r_{N,i} = ^{14}r_i \left[ 1 - 2 \left( \frac{\delta^{13}\text{C}_i + 25}{1000} \right) \right], \quad (\text{A1})$$

where the two terms in the numerator in parentheses are in permil, and

$$\Delta^{14}\text{C}_i = \left( \frac{^{14}r_{N,i}}{^{14}r_{\text{std}}} - 1 \right) 1000. \quad (\text{A2})$$

Deviations between this correction and the actual impact of fractionation on  $^{14}\text{C}$  occur under non-steady-state conditions. More importantly, radioactive decay in the ocean results in a net transfer of  $^{14}\text{C}$  into the ocean, unlike the case for  $^{13}\text{C}$ , and this net  $^{14}\text{C}$  flux is not corrected for fractionation. In OMIP, we simplify equations and avoid small numerical values by defining  $^{14}r' = ^{14}r / ^{14}r_{\text{std}}$  (i.e., compare Eq. (A2) with Eq. (30)). This normalization is further discussed in Sects. 2.5.3 and 2.5.4 (see in particular Eqs. 19 and 29).

Thus OMIP simulates a  $^{14}\text{C}$  concentration that is (1) fractionation corrected and (2) normalized by dividing  $^{14}r$  by  $^{14}r_{\text{std}}$ . These corrections must be removed to convert modeled concentrations into number of atoms or moles of  $^{14}\text{C}$ . Thus, we rearrange Eq. (A1) while multiplying by the common denominator (C) of both its  $^{14}r$  values and then we multiply by  $^{14}r_{\text{std}}$ , yielding

$$^{14}\text{C} = \left( ^{14}\text{C}_{\text{model}} / \left[ 1 - 2 \left( \frac{(\delta^{13}\text{C} + 25)}{1000} \right) \right] \right) ^{14}r_{\text{std}}. \quad (\text{A3})$$

Here we neglect that the  $\delta^{13}\text{C}$  of the standard material ( $-19\text{‰}$ , Karlen et al., 1965) differs from that of ocean water ( $-1$  to  $2\text{‰}$ ) because the resulting bias in computed  $^{14}\text{C}$  is only  $0.02\text{‰}$ .

Now let us use Eq. (A3) to compute corrections for the preindustrial ocean and atmosphere by plugging in their estimated  $\delta^{13}\text{C}$  values. For the preindustrial ocean, we assume that  $\delta^{13}\text{C}$  was around  $2\text{‰}$  in surface waters and  $0\text{‰}$  in the deep ocean, a difference attributable to biological fractionation. Inserting those numbers into Eq. (A3) and simplifying, we thus have

$$^{14}\text{C}_S \approx ^{14}\text{C}_{\text{model},S} \left( 1 + \frac{54}{1000} \right) ^{14}r_{\text{std}}, \quad (\text{A4a})$$

$$^{14}\text{C}_D \approx ^{14}\text{C}_{\text{model},D} \left( 1 + \frac{50}{1000} \right) ^{14}r_{\text{std}}, \quad (\text{A4b})$$

where the subscripts “S” and “D” indicate surface and deep waters. Thus, there is a correction of  $54\text{‰}$  for the surface ocean and  $50\text{‰}$  for the deep ocean. For the preindustrial atmosphere, using the same approach with its assumed  $\delta^{13}\text{C}$  of  $-6.4\text{‰}$ , we find

$$^{14}\text{C}_A \approx ^{14}\text{C}_{\text{model},A} \left( 1 + \frac{37}{1000} \right) ^{14}r_{\text{std}}. \quad (\text{A5})$$

Thus, the  $^{14}\text{C}_A$  correction to switch from model to conventional units for the atmosphere is about  $37\text{‰}$ .

Turning to the gas exchange, in the model formulation the related change in the atmospheric  $^{14}\text{C}$  inventory is calculated by removing the net air-to-sea flux  $F_{^{14}\text{CO}_2^{\text{abio}}}$  and adding

that to the ocean  $^{14}\text{C}$  inventory. To convert this modeled air–sea flux into atomic units, we use the same correction as for the modeled concentrations because the change in inventory is proportional to the change in concentrations. The difference between the atmospheric and oceanic corrections ( $54 - 37 = 17\text{‰}$ ) is related to the equilibrium fractionation factor for air–sea transfer, i.e.,  $8\text{--}9\text{‰}$  for  $^{13}\text{C}$  and double that for  $^{14}\text{C}$ . In the model, the impact of fractionation on the net (non-zero) radiocarbon transfer is not taken explicitly into account, giving rise to this inconsistency even under equilibrium conditions where a climatological average flux replaces the ocean sink by radioactive decay.

In the OMIP simulations, atmospheric radiocarbon is prescribed and forces the ocean. The ocean radiocarbon inventory changes in response to this forcing. Thus, a correction of about  $+50\text{‰}$  (Eqs. A4a and A4b) is needed to convert ocean  $^{14}\text{C}$  concentrations and net air–sea  $^{14}\text{C}$  fluxes from model units into molar units. Hence for concentrations,

$$^{14}\text{C}_{\text{T}} = ^{14}\text{C}_{\text{T,model}}^{\text{abio}} \times 1.05 \times 1.170 \times 10^{-12}, \quad (\text{A6})$$

and for fluxes,

$$F_{^{14}\text{CO}_2} = F_{^{14}\text{CO}_2,\text{model}}^{\text{abio}} \times 1.05 \times 1.170 \times 10^{-12}. \quad (\text{A7})$$

In both Eqs. (A6) and (A7), units on the left-hand side are in terms of  $\text{mol } ^{14}\text{C}$ , while those for the first term on the right-hand side are model units (*normalized* and *fractionation-corrected*  $\text{mol } ^{14}\text{C}$ ).

**The Supplement related to this article is available online at <https://doi.org/10.5194/gmd-10-2169-2017-supplement>.**

*Competing interests.* The authors declare that they have no conflict of interest.

*Acknowledgements.* Thanks to two anonymous reviewers and the editor (G. Munhoven) for comments. J. C. Orr and L. Bopp were supported by the EU H2020 CRESCENDO project (grant 641816). J. L. Bullister was supported by the NOAA Climate Program Office – this is PMEL contribution no. 476. H. Graven was supported by an EU Marie Curie Career Integration Grant. A. Mouchet benefited from an EU H2020 Marie Curie project (grant 660893). R. G. Najjar was supported by NASA's Ocean Biology and Biogeochemistry Program and NASA's Interdisciplinary Science Program. F. Joos was supported by the Swiss National Science Foundation. The National Center for Atmospheric Research (NCAR) is sponsored by the US National Science Foundation. J.-M. Epitalon modified *mocsy* to allow for optional input of conservative temperature and absolute salinity.

Edited by: G. Munhoven

Reviewed by: two anonymous referees

## References

- Audi, G., Bersillon, O., Blachot, J., and Wapstra, A. H.: The NUBASE evaluation of nuclear and decay properties, *Nucl. Phys. A*, 729, 3–128, 2003.
- Aumont, O. and Bopp, L.: Globalizing results from ocean in situ iron fertilization studies, *Global Biogeochem. Cy.*, 20, GB2017, <https://doi.org/10.1029/2005GB002591>, 2006.
- Aumont, O., Orr, J. C., Jamous, D., Monfray, P., Marti, O., and Madec, G.: A degradation approach to accelerate simulations to steady state in a 3-D tracer transport model of the global ocean, *Clim. Dynam.*, 14, 101–116, 1998.
- Aumont, O., Le Quéré, C., and Orr, J. C.: NOCES Interannual HOWTO. Internal NOCES/OCMIP report, LSCE/CEA Saclay, Gif-sur-Yvette, France, 2nd Edn., <http://ocmip5.ipsl.jussieu.fr/OCMIP/phase3/simulations/NOCES/HOWTO-NOCES.html>, 2004.
- Bacastow, R. and Maier-Reimer, E.: Ocean-circulation model of the carbon cycle, *Clim. Dynam.*, 4, 95–125, 1990.
- Bé, M., Chisté, V., Dulieu, C., Mougeot, X., Chechev, V., Kondev, F., Nichols, A., Huang, X., and Wang, B.: Table of Radionuclides (Comments on evaluations), Monographie BIPM-5, Vol. 7, Bureau International des Poids et Mesure, Pavillon de Breteuil, Sèvres, France, 2013.
- Bopp, L., Resplandy, L., Orr, J. C., Doney, S. C., Dunne, J. P., Gehlen, M., Halloran, P., Heinze, C., Ilyina, T., Séférián, R., Tjiputra, J., and Vichi, M.: Multiple stressors of ocean ecosystems in the 21st century: projections with CMIP5 models, *Biogeosciences*, 10, 6225–6245, <https://doi.org/10.5194/bg-10-6225-2013>, 2013.
- Broecker, W. and Peng, T.: Tracers in the sea, Eldigio, Lamont-Doherty, Palisades, NY, 691 pp., 1982.
- Broecker, W., Peacock, S., Walker, S., Weiss, R., Fahrback, E., Schröder, M., Mikolajewicz, U., Heinze, C., Key, R., Peng, T.-H., and Rubin, S.: How much deep water is formed in the Southern Ocean?, *J. Geophys. Res.*, 103, C8, 15833–15843, 1998.
- Broecker, W. S. and Olson, E. A.: Lamont radiocarbon measurements VIII, *Radiocarbon*, 3, 176–204, 1961.
- Broecker, W. S. and Peng, T.-H.: Gas exchange rates between air and sea, *Tellus*, 26, 21–35, 1974.
- Bullister, J.: Atmospheric Histories (1765–2015) for CFC-11, CFC-12, CFC-113, CCl<sub>4</sub>, SF<sub>6</sub> and N<sub>2</sub>O, Carbon Dioxide Information Analysis Center, Oak Ridge National Laboratory, US Department of Energy, Oak Ridge, Tennessee, [http://cdiac.ornl.gov/ftp/oceans/CFC\\_ATM\\_Hist/CFC\\_ATM\\_Hist\\_2015](http://cdiac.ornl.gov/ftp/oceans/CFC_ATM_Hist/CFC_ATM_Hist_2015), [https://doi.org/10.3334/CDIAC/otg.CFC\\_ATM\\_Hist\\_2015](https://doi.org/10.3334/CDIAC/otg.CFC_ATM_Hist_2015), 2015.
- Bullister, J. L., Wisegarver, D. P., and Menzia, F. A.: The solubility of sulfur hexafluoride in water and seawater, *Deep-Sea Res. Pt. I*, 49, 175–187, 2002.
- Craig, H.: Isotopic standards for carbon and oxygen and correction factors for mass-spectrometric analysis of carbon dioxide, *Geochim. Cosmochim. Acta*, 12, 133–149, 1957.
- Dickson, A. G.: The carbon dioxide system in seawater: equilibrium chemistry and measurements, in: Guide to best practices for ocean acidification research and data reporting, edited by: Riebesell, U., Fabry, V. J., Hansson, L., and Gattuso, J.-P., Publications Office of the European Union, 17–40, 2010.
- Dickson, A. G., Sabine, C. L., and Christian, J. R.: Guide to best practices for ocean CO<sub>2</sub> measurements, PICES Special Publication 3, 191 pp., <http://aquaticcommons.org/1443/>, 2007.
- Drügkenky, E. and Tans, P.: Trends in atmospheric carbon dioxide, National Oceanic & Atmospheric Administration, Earth System Research Laboratory (NOAA/ESRL), available at: <http://www.esrl.noaa.gov/gmd/ccgg/trends>, 2016.
- Doney, S., Lindsay, K., Caldeira, K., Campin, J.-M., Drange, H., Dutay, J.-C., Follows, M., Gao, Y., Gnanadesikan, A., Gruber, N., Ishida, A., Joos, F., Madec, G., Maier-Reimer, E., Marshall, J., Matear, R., Monfray, P., Mouchet, A., Najjar, R., Orr, J., Plattner, G.-K., Sarmiento, J., Schlitzer, R., Slater, R., Totterdell, I., Weirig, M.-F., Yamanaka, Y., and Yool, A.: Evaluating global ocean carbon models: the importance of realistic physics, *Global Biogeochem. Cy.*, 18, GB3017, <https://doi.org/10.1029/2003GB002150>, 2004.
- Dufour, C. O., Sommer, J. L., Gehlen, M., Orr, J. C., Molines, J.-M., Simeon, J., and Barnier, B.: Eddy compensation and controls of the enhanced sea-to-air CO<sub>2</sub> flux during positive phases of the Southern Annular Mode, *Global Biogeochem. Cy.*, 27, 950–961, <https://doi.org/10.1002/gbc.20090>, 2013.
- Dutay, J.-C., Bullister, J., Doney, S. C., Orr, J. C., Najjar, R. G., Caldeira, K., Campin, J.-M., Drange, H., Follows, M., Gao, Y., Gruber, N., Hecht, M. W., Ishida, A., Joos, F., Lindsay, K., Madec, G., Maier-Reimer, E., Marshall, J. C., Matear, R., Monfray, P., Mouchet, A., Plattner, G. K., Sarmiento, J. L., Schlitzer, R., Slater, R. D., Totterdell, I. J., Weirig, M.-F., Yamanaka, Y., and Yool, A.: Evaluation of ocean model ventilation with CFC-11: comparison of 13 global ocean models, *Ocean Model.*, 4, 89–120, 2002.

- Dutay, J.-C., Jean-Baptiste, P., Campin, J.-M., Ishida, A., Maier-Reimer, E., Matear, R., Mouchet, A., Totterdell, I., Yamanaka, Y., Rodgers, K., Madec, G., and Orr, J.: Evaluation of OCMIP-2 ocean models' deep circulation with mantle helium-3, *J. Marine Syst.*, 48, 15–36, <https://doi.org/10.1016/j.jmarsys.2003.05.010>, 2004.
- Eyring, V., Bony, S., Meehl, G. A., Senior, C. A., Stevens, B., Stouffer, R. J., and Taylor, K. E.: Overview of the Coupled Model Intercomparison Project Phase 6 (CMIP6) experimental design and organization, *Geosci. Model Dev.*, 9, 1937–1958, <https://doi.org/10.5194/gmd-9-1937-2016>, 2016.
- Garcia, H. E. and Gordon, L. I.: Oxygen solubility in seawater: Better fitting equations, *Limnol. Oceanogr.*, 37, 1307–1312, 1992.
- Garcia, H. E., Locarnini, R. A., Boyer, T. P., Antonov, J. I., Baranova, O., Zweng, M., Reagan, J., and Johnson, D.: World Ocean Atlas 2013, in: Dissolved Oxygen, Apparent Oxygen Utilization, and Oxygen Saturation, Vol. 3, edited by: Levitus, S. and Mishonov, A., Atlas NESDIS 75, NOAA, US Government Printing Office, Washington, DC, 27 pp., 2014a.
- Garcia, H. E., Locarnini, R. A., Boyer, T. P., Antonov, J. I., Baranova, O., Zweng, M., Reagan, J., and Johnson, D.: World Ocean Atlas 2013, Dissolved Inorganic Nutrients (phosphate, nitrate, silicate), Vol. 4, edited by: Levitus, S. and Mishonov, A., Atlas NESDIS 76, NOAA, US Government Printing Office, Washington, DC, 25 pp., 2014b.
- Godwin, H.: Half-life of radiocarbon, *Nature*, 195, 984 pp., 1962.
- Graven, H. D., Gruber, N., Key, R., Khatiwala, S., and Giraud, X.: Changing controls on oceanic radiocarbon: New insights on shallow-to-deep ocean exchange and anthropogenic CO<sub>2</sub> uptake, *J. Geophys. Res.*, 117, C10005, <https://doi.org/10.1029/2012JC008074>, 2012.
- Griffies, S. M., Danabasoglu, G., Durack, P. J., Adcroft, A. J., Balaji, V., Böning, C. W., Chassignet, E. P., Curchitser, E., Deshayes, J., Drange, H., Fox-Kemper, B., Gleckler, P. J., Gregory, J. M., Haak, H., Hallberg, R. W., Heimbach, P., Hewitt, H. T., Holland, D. M., Ilyina, T., Jungclaus, J. H., Komuro, Y., Krasting, J. P., Large, W. G., Marsland, S. J., Masina, S., McDougall, T. J., Nurser, A. J. G., Orr, J. C., Pirani, A., Qiao, F., Stouffer, R. J., Taylor, K. E., Treguier, A. M., Tsujino, H., Uotila, P., Valdivieso, M., Wang, Q., Winton, M., and Yeager, S. G.: OMIP contribution to CMIP6: experimental and diagnostic protocol for the physical component of the Ocean Model Intercomparison Project, *Geosci. Model Dev.*, 9, 3231–3296, <https://doi.org/10.5194/gmd-9-3231-2016>, 2016.
- Hansell, D. A., Carlson, C. A., Repeta, D. J., and Schlitzer, R.: Dissolved organic matter in the ocean: A controversy stimulates new insights, *Oceanography*, 22, 202–211, 2009.
- Jahn, A., Lindsay, K., Giraud, X., Gruber, N., Otto-Bliesner, B. L., Liu, Z., and Brady, E. C.: Carbon isotopes in the ocean model of the Community Earth System Model (CESM1), *Geosci. Model Dev.*, 8, 2419–2434, <https://doi.org/10.5194/gmd-8-2419-2015>, 2015.
- Jones, C. D., Arora, V., Friedlingstein, P., Bopp, L., Brovkin, V., Dunne, J., Graven, H., Hoffman, F., Ilyina, T., John, J. G., Jung, M., Kawamiya, M., Koven, C., Pongratz, J., Raddatz, T., Randerson, J. T., and Zaehle, S.: C4MIP – The Coupled Climate-Carbon Cycle Model Intercomparison Project: experimental protocol for CMIP6, *Geosci. Model Dev.*, 9, 2853–2880, <https://doi.org/10.5194/gmd-9-2853-2016>, 2016.
- Joos, F., Orr, J. C., and Siegenthaler, U.: Ocean carbon transport in a box-diffusion versus a general circulation model, *J. Geophys. Res.*, 102, 12367–12388, 1997.
- Karlen, I., Olsson, I., Kallberg, P., and Kilicci, S.: Absolute determination of the activity of two C-14 dating standards, *Arkiv Geofysik.*, 4, 465–471, 1965.
- Keeling, C. D., Piper, S. C., Bacastow, R. B., Wahlen, M., Whorf, T. P., Heimann, M., and Meijer, H. A.: Exchanges of Atmospheric CO<sub>2</sub> and <sup>13</sup>CO<sub>2</sub> with the Terrestrial Biosphere and Oceans from 1978 to 2000, I. Global Aspects, SIO Reference Series 01-06, Scripps Institution of Oceanography, San Diego, 2001.
- Key, R. M., Sabine, C. L., Lee, K., Wanninkhof, R., Bullister, J., Feely, R. A., Millero, F. J., Mordy, C., and Peng, T.-H.: A Global ocean carbon climatology: Results from Global Data Analysis Project (GLODAP), *Global Biogeochem. Cy.*, 18, GB4031, <https://doi.org/10.1029/2004GB002247>, 2004.
- Khatiwala, S.: Fast spin up of ocean biogeochemical models using matrix-free Newton–Krylov, *Ocean Model.*, 23, 121–129, 2008.
- Kwiatkowski, L., Yool, A., Allen, J. I., Anderson, T. R., Barciela, R., Buitenhuis, E. T., Butenschön, M., Enright, C., Halloran, P. R., Le Quéré, C., de Mora, L., Racault, M.-F., Sinha, B., Totterdell, I. J., and Cox, P. M.: iMarNet: an ocean biogeochemistry model intercomparison project within a common physical ocean modelling framework, *Biogeosciences*, 11, 7291–7304, <https://doi.org/10.5194/bg-11-7291-2014>, 2014.
- Large, W. G. and Yeager, S. G.: The global climatology of an inter-annually varying air–sea flux data set, *Clim. Dynam.*, 33, 341–364, 2009.
- Lauvset, S. K., Key, R. M., Olsen, A., van Heuven, S., Velo, A., Lin, X., Schirnick, C., Kozyr, A., Tanhua, T., Hoppema, M., Jutterström, S., Steinfeldt, R., Jeansson, E., Ishii, M., Perez, F. F., Suzuki, T., and Watelet, S.: A new global interior ocean mapped climatology: the 1° × 1° GLODAP version 2, *Earth Syst. Sci. Data*, 8, 325–340, <https://doi.org/10.5194/essd-8-325-2016>, 2016.
- Levin, I., Naegler, T., Kromer, B., Diehl, M., Francey, R. J., Gomez-Pelaez, A. J., Steele, L., Wagenbach, D., Weller, R., and Worthy, D. E.: Observations and modelling of the global distribution and long-term trend of atmospheric <sup>14</sup>CO<sub>2</sub>, *Tellus B*, 62, 26–46, 2010.
- Li, X. and Primeau, F. W.: A fast Newton–Krylov solver for seasonally varying global ocean biogeochemistry models, *Ocean Model.*, 23, 13–20, 2008.
- Lovenduski, N. S., McKinley, G. A., Fay, A. R., Lindsay, K., and Long, M. C.: Partitioning uncertainty in ocean carbon uptake projections: Internal variability, emission scenario, and model structure, *Global Biogeochem. Cy.*, 30, 1276–1287, <https://doi.org/10.1002/2016GB005426>, 2016.
- Matsumoto, K., Sarmiento, J. L., Key, R. M., Aumont, O., Bullister, J. L., Caldeira, K., Campin, J.-M., Doney, S. C., Drange, H., Dutay, J.-C., Follows, M., Gao, Y., Gnanadesikan, A., Gruber, N., Ishida, A., Joos, F., Lindsay, K., Maier-Reimer, E., Marshall, J. C., Matear, R. J., Monfray, P., Mouchet, A., Najjar, R., Plattner, G.-K., Schlitzer, R., Slater, R., Swathi, P. S., Totterdell, I. J., Weirig, M.-F., Yamanaka, Y., Yool, A., and Orr, J. C.: Evaluation of ocean carbon cycle models with data-based metrics, *Geophys. Res. Lett.*, 31, L07303, <https://doi.org/10.1029/2003GL018970>, 2004.



- Meinshausen, M., Vogel, E., Nauels, A., Lorbacher, K., Meinshausen, N., Etheridge, D., Fraser, P., Montzka, S. A., Rayner, P., Trudinger, C., Krummel, P., Beyerle, U., Cannadell, J. G., Daniel, J. S., Enting, I., Law, R. M., O'Doherty, S., Prinn, R. G., Reimann, S., Rubino, M., Velders, G. J. M., Vollmer, M. K., and Weiss, R.: Historical greenhouse gas concentrations, *Geosci. Model Dev. Discuss.*, <https://doi.org/10.5194/gmd-2016-169>, in review, 2016.
- Merlis, T. M. and Khatiwala, S.: Fast dynamical spin-up of ocean general circulation models using Newton–Krylov methods, *Ocean Model.*, 21, 97–105, 2008.
- Montzka, S. A., Fraser, P. J., Butler, J. H., Cunnold, D. M., Daniel, J. S., Derwent, R. G., Lal, S., McCulloch, A., Oram, D. E., Reeves, C. E., Sanhueza, E., Steele, L. P., Velders, G. J. M., Weiss, R. F., and Zander, R. J.: Scientific Assessment of Ozone Depletion, Vol. 47, Chapter 1: Controlled substances and other source gases, World Meteorol. Organ., Geneva, Switzerland, 2003.
- Mook, W.:  $^{13}\text{C}$  in atmospheric  $\text{CO}_2$ , *Neth. J. Sea Res.*, 20, 211–223, 1986.
- Mouchet, A.: The ocean bomb radiocarbon inventory revisited, *Radiocarbon*, 55, 1580–1594, 2013.
- Munhoven, G.: Mathematics of the total alkalinity–pH equation – pathway to robust and universal solution algorithms: the SolveSAPHE package v1.0.1, *Geosci. Model Dev.*, 6, 1367–1388, <https://doi.org/10.5194/gmd-6-1367-2013>, 2013.
- Naegler, T.: Reconciliation of excess  $^{14}\text{C}$ -constrained global  $\text{CO}_2$  piston velocity estimates, *Tellus B*, 61, 372–384, <https://doi.org/10.1111/j.1600-0889.2008.00408.x>, 2009.
- Najjar, R. and Orr, J.: Design of OCMIP-2 simulations of chlorofluorocarbons, the solubility pump and common biogeochemistry, Internal OCMIP Report, LSCE/CEA Saclay, Gif-sur-Yvette, France, <http://ocmip5.ipsl.fr/documentation/OCMIP/phase2/simulations/design.ps>, 1998.
- Najjar, R. and Orr, J. C.: Biotic-HOWTO. Internal OCMIP Report, LSCE/CEA Saclay, Gif-sur-Yvette, France, 15 pp., <http://ocmip5.ipsl.jussieu.fr/OCMIP/phase2/simulations/Biotic/HOWTO-Biotic.html>, 1999.
- Najjar, R. G., Jin, X., Louanchi, F., Aumont, O., Caldeira, K., Doney, S. C., Dutay, J.-C., Follows, M., Gruber, N., Joos, F., Lindsay, K., Maier-Reimer, E., Matear, R. J., Matsumoto, K., Monfray, P., Mouchet, A., Orr, J. C., Plattner, G.-K., Sarmiento, J. L., Schlitzer, R., Slater, R. D., Yamanaka, Y., Weirig, M.-F. and Yool, A.: Impact of circulation on export production, dissolved organic matter, and dissolved oxygen in the ocean: Results from Phase II of the Ocean Carbon-cycle Model Intercomparison Project (OCMIP-2), *Global Biogeochem. Cy.*, 21, GB3007, <https://doi.org/10.1029/2006GB002857>, 2007.
- Oliver, K. I. C., Hoogakker, B. A. A., Crowhurst, S., Henderson, G. M., Rickaby, R. E. M., Edwards, N. R., and Elderfield, H.: A synthesis of marine sediment core  $\delta^{13}\text{C}$  data over the last 150 000 years, *Clim. Past*, 6, 645–673, <https://doi.org/10.5194/cp-6-645-2010>, 2010.
- Olsen, A., Key, R. M., van Heuven, S., Lauvset, S. K., Velo, A., Lin, X., Schirnick, C., Kozyr, A., Tanhua, T., Hoppema, M., Jutterström, S., Steinfeldt, R., Jeansson, E., Ishii, M., Pérez, F. F., and Suzuki, T.: The Global Ocean Data Analysis Project version 2 (GLODAPv2) – an internally consistent data product for the world ocean, *Earth Syst. Sci. Data*, 8, 297–323, <https://doi.org/10.5194/essd-8-297-2016>, 2016.
- Orr, J. C. and Epitalon, J.-M.: Improved routines to model the ocean carbonate system: mocsy 2.0, *Geosci. Model Dev.*, 8, 485–499, <https://doi.org/10.5194/gmd-8-485-2015>, 2015.
- Orr, J. C., Dutay, J.-C., Najjar, R., Bullister, J., and Brockmann, P.: CFC-HOWTO. Internal OCMIP Report, LSCE/CEA Saclay, Gif-sur-Yvette, France, 12 pp., <http://ocmip5.ipsl.jussieu.fr/OCMIP/phase2/simulations/CFC/HOWTO-CFC.html>, 1999a.
- Orr, J. C., Najjar, R., Sabine, C. L., and Joos, F.: Abiotic-HOWTO, Internal OCMIP Report, LSCE/CEA Saclay, Gif-sur-Yvette, France, 25 pp., <http://ocmip5.ipsl.jussieu.fr/OCMIP/phase2/simulations/Abiotic/HOWTO-Abiotic.html>, 1999b.
- Orr, J. C., Monfray, P., Maier-Reimer, E., Mikolajewicz, U., Palmer, J., Taylor, N. K., Toggweiler, J. R., Sarmiento, J. L., Quéré, C. L., Gruber, N., Sabine, C. L., Key, R. M., and Boutin, J.: Estimates of anthropogenic carbon uptake from four three-dimensional global ocean models, *Global Biogeochem. Cy.*, 15, 43–60, 2001.
- Orr, J. C., Fabry, V. J., Aumont, O., Bopp, L., Doney, S. C., Feely, R. A., Gnanadesikan, A., Gruber, N., Ishida, A., Joos, F., Key, R. M., Lindsay, K., Maier-Reimer, E., Matear, R., Monfray, P., Mouchet, A., Najjar, R. G., Plattner, G.-K., Rodgers, K. B., Sabine, C. L., Sarmiento, J. L., Schlitzer, R., Slater, R. D., Totterdell, I. J., Weirig, M.-F., Yamanaka, Y., and Yool, A.: Anthropogenic ocean acidification over the twenty-first century and its impact on calcifying organisms, *Nature*, 437, 681–686, <https://doi.org/10.1038/nature04095>, 2005.
- Orr, J. C., Epitalon, J.-M., and Gattuso, J.-P.: Comparison of ten packages that compute ocean carbonate chemistry, *Biogeochemistry*, 12, 1483–1510, <https://doi.org/10.5194/bg-12-1483-2015>, 2015.
- Peacock, S.: Debate over the ocean bomb radiocarbon sink: Closing the gap, *Global Biogeochem. Cy.*, 18, GB2022, <https://doi.org/10.1029/2003GB002211>, 2004.
- Penduff, T., Juza, M., Barnier, B., Zika, J., Dewar, W. K., Treguier, A.-M., Molines, J.-M., and Audiffren, N.: Sea level expression of intrinsic and forced ocean variabilities at interannual time scales, *J. Climate*, 24, 5652–5670, 2011.
- Quay, P., Sonnerup, R., Westby, T., Stutsman, J., and McNichol, A.: Changes in the  $^{13}\text{C}/^{12}\text{C}$  of dissolved inorganic carbon in the ocean as a tracer of anthropogenic  $\text{CO}_2$  uptake, *Global Biogeochem. Cy.*, 17, 1004, <https://doi.org/10.1029/2001GB001817>, 2003.
- Quay, P. D., Tilbrook, B., and Wong, C.: Oceanic uptake of fossil fuel  $\text{CO}_2$ : Carbon-13 evidence, *Science*, 256, 74–79, 1992.
- Raynaud, S., Orr, J. C., Aumont, O., Rodgers, K. B., and Yiou, P.: Interannual-to-decadal variability of North Atlantic air-sea  $\text{CO}_2$  fluxes, *Ocean Sci.*, 2, 43–60, <https://doi.org/10.5194/os-2-43-2006>, 2006.
- Redfield, A. C., Ketchum, B. H., and Richards, F.: The influence of organisms on the composition of sea water, in: *The Sea*, edited by: Hill, M. N., Wiley-Interscience, New York, 2, 26–77, 1963.
- Rigby, M., Prinn, R. G., O'Doherty, S., Montzka, S. A., McCulloch, A., Harth, C. M., Mühle, J., Salameh, P. K., Weiss, R. F., Young, D., Simmonds, P. G., Hall, B. D., Dutton, G. S., Nance, D., Mondeel, D. J., Elkins, J. W., Krummel, P. B., Steele, L. P., and Fraser, P. J.: Re-evaluation of the lifetimes of the major CFCs and  $\text{CH}_3\text{CCl}_3$  using atmospheric trends, *Atmos. Chem. Phys.*, 13, 2691–2702, <https://doi.org/10.5194/acp-13-2691-2013>, 2013.

- Rodgers, K. B., Aumont, O., Madec, G., Menkes, C., Blanke, B., Monfray, P., Orr, J. C., and Schrag, D. P.: Radiocarbon as a thermocline proxy for the eastern equatorial Pacific, *Geophys. Res. Lett.*, 31, L14314, <https://doi.org/10.1029/2004GL019764>, 2004.
- Roullet, G. and Madec, G.: Salt conservation, free surface, and varying levels: A new formulation for ocean general circulation models, *J. Geophys. Res.*, 105, 23927–23942, <https://doi.org/10.1029/2000JC900089>, 2000.
- Rubino, M., Etheridge, D. M., Trudinger, C. M., Allison, C. E., Battle, M. O., Langenfelds, R. L., Steele, L. P., Curran, M., Bender, M., White, J. W. C., Jenk, T. M., Blunier, T., and Francey, R. J.: A revised 1000 year atmospheric  $\delta^{13}\text{C}$ -CO<sub>2</sub> record from Law Dome and South Pole, Antarctica, *J. Geophys. Res.-Atmos.*, 118, 8482–8499, <https://doi.org/10.1002/jgrd.50668>, 2013.
- Sarmiento, J. L., Monfray, P., Maier-Reimer, E., Aumont, O., Mur-nane, R., and Orr, J. C.: Sea-air CO<sub>2</sub> fluxes and carbon transport: A comparison of three ocean general circulation models, *Global Biogeochem. Cy.*, 14, 1267–1281, 2000.
- Schmitt, J., Schneider, R., Elsig, J., Leuenberger, D., Laurantou, A., Chappellaz, J., Köhler, P., Joos, F., Stocker, T. F., Leuenberger, M., et al.: Carbon isotope constraints on the deglacial CO<sub>2</sub> rise from ice cores, *Science*, 336, 711–714, 2012.
- Schmittner, A., Gruber, N., Mix, A. C., Key, R. M., Tagliabue, A., and Westberry, T. K.: Biology and air-sea gas exchange controls on the distribution of carbon isotope ratios ( $\delta^{13}\text{C}$ ) in the ocean, *Biogeosciences*, 10, 5793–5816, <https://doi.org/10.5194/bg-10-5793-2013>, 2013.
- Séférian, R., Gehlen, M., Bopp, L., Resplandy, L., Orr, J. C., Marti, O., Dunne, J. P., Christian, J. R., Doney, S. C., Ilyina, T., Lindsay, K., Halloran, P. R., Heinze, C., Segschneider, J., Tjiputra, J., Aumont, O., and Romanou, A.: Inconsistent strategies to spin up models in CMIP5: implications for ocean biogeochemical model performance assessment, *Geosci. Model Dev.*, 9, 1827–1851, <https://doi.org/10.5194/gmd-9-1827-2016>, 2016.
- Sweeney, C., Gloor, E., Jacobson, A. R., Key, R. M., McKinley, G., Sarmiento, J. L., and Wanninkhof, R.: Constraining global air-sea gas exchange for CO<sub>2</sub> with recent bomb <sup>14</sup>C measurements, *Global Biogeochem. Cy.*, 21, GB2015, <https://doi.org/10.1029/2006GB002784>, 2007.
- Tagliabue, A. and Bopp, L.: Towards understanding global variability in ocean carbon-13, *Global Biogeochem. Cy.*, 22, GB1025, <https://doi.org/10.1029/2007GB003037>, 2008.
- Tagliabue, A., Aumont, O., DeAth, R., Dunne, J. P., Dutkiewicz, S., Galbraith, E., Misumi, K., Moore, J. K., Ridgwell, A., Sherman, E., Stock, C., Vichi, M., Völker, C., and Yool, A.: How well do global ocean biogeochemistry models simulate dissolved iron distributions?, *Global Biogeochem. Cy.*, 30, 149–174, <https://doi.org/10.1002/2015GB005289>, 2016.
- Toggweiler, J. R., Dixon, K., and Bryan, K.: Simulations of radio-carbon in a coarse resolution world ocean model: 1. Steady state prebomb distributions, *J. Geophys. Res.*, 94, 8217–8242, 1989a.
- Toggweiler, J. R., Dixon, K., and Bryan, K.: Simulations of radio-carbon in a coarse resolution world ocean model: 2. Distributions of bomb-produced carbon 14, *J. Geophys. Res.*, 94, 8243–8264, 1989b.
- Walker, S. J., Weiss, R. F., and Salameh, P. K.: Reconstructed histories of the annual mean atmospheric mole fractions for the halocarbons CFC-11 CFC-12, CFC-113, and carbon tetrachloride, *J. Geophys. Res.*, 105, 14285–14296, <https://doi.org/10.1029/1999JC900273>, 2000.
- Wanninkhof, R.: Relationship between wind speed and gas exchange over the ocean, *J. Geophys. Res.*, 97, 7373–7382, 1992.
- Wanninkhof, R.: Relationship between wind speed and gas exchange over the ocean revisited, *Limnol. Oceanogr.-Meth.*, 12, 351–362, 2014.
- Warner, M. J. and Weiss, R. F.: Solubilities of chlorofluorocarbons 11 and 12 in water and seawater, *Deep-Sea Res. Pt. A.*, 32, 1485–1497, 1985.
- Waugh, D. W., Hall, T. M., and Haine, T. W. N.: Relationship among tracer ages, *J. Geophys. Res.*, 108, 3138, <https://doi.org/10.1029/2002JC001325>, 2003.
- Weiss, R. F.: Carbon dioxide in water and seawater: the solubility of a non-ideal gas, *Mar. Chem.*, 2, 203–215, 1974.
- Weiss, R. F. and Price, B. A.: Nitrous oxide solubility in water and seawater, *Mar. Chem.*, 8, 347–359, 1980.
- Wolf-Gladrow, D. A., Zeebe, R. E., Klaas, C., Körtzinger, A., and Dickson, A. G.: Total alkalinity: The explicit conservative expression and its application to biogeochemical processes, *Mar. Chem.*, 106, 287–300, 2007.
- Yool, A., Oschlies, A., Nurser, A. J. G., and Gruber, N.: A model-based assessment of the TrOCA approach for estimating anthropogenic carbon in the ocean, *Biogeosciences*, 7, 723–751, <https://doi.org/10.5194/bg-7-723-2010>, 2010.
- Zhang, J., Quay, P. D., and Wilbur, D. O.: Carbon isotope fractionation during gas-water exchange and dissolution of CO<sub>2</sub>, *Geochim. Cosmochim. Ac.*, 59, 107–114, 1995.